IEEE Access
Multidisciplinary | Rapid Review | Open Access Journal

Received May 7, 2020, accepted May 14, 2020, date of publication May 18, 2020, date of current version June 2, 2020.

Digital Object Identifier 10.1109/ACCESS.2020.2995435

Performance Analysis of Reconfigurable Intelligent Surface-Assisted Wireless Systems and Comparison With Relaying

ALEXANDROS-APOSTOLOS A. BOULOGEORGOS, (Senior Member, IEEE), AND ANGELIKI ALEXIOU, (Member, IEEE)
Department of Digital Systems, University of Piraeus, 18534 Piraeus, Greece

Corresponding author: Alexandros-Apostolos A. Boulogeorgos (al.boulogeorgos@ieee.org)

This work was supported by the European Commission's Horizon 2020 Research and Innovation Programme under Agreement 871464 (ARIADNE).

ABSTRACT In this paper, we provide the theoretical framework for the performance comparison of reconfigurable intelligent surfaces (RISs) and amplify-and-forward (AF) relaying wireless systems. In particular, after statistically characterizing the end-to-end (e2e) wireless channel coefficient of the RIS-assisted wireless system, in terms of probability density function (PDF) and cumulative density function (CDF), we extract novel closed-form expressions for the instantaneous and average e2e signal-to-noise ratio (SNR) for both the RIS-assisted and AF-relaying wireless systems. Building upon these expressions, we derive the diversity gain of the RIS-assisted wireless system as well as the outage probability (OP) and symbol error rate (SER) for a large variety of Gray-mapped modulation schemes of both systems under investigation. Additionally, the diversity order of the RIS-assisted wireless system is presented as well as the ergodic capacity (EC) of both the RIS-assisted and AF-relaying wireless systems. Likewise, high-SNR and high-number of metasurfaces (MS) approximations for the SER and EC for the RIS-assisted wireless system are reported. Finally, for the sake of completeness, the special case in which the RIS is equipped with only one MS is also investigated. For this case, the instantaneous and average e2e SNR are derived, as well as the OP, SER and EC. Our analysis is verified through respective Monte Carlo simulations, which reveal the accuracy of the presented theoretical framework. Moreover, our results highlight that, in general, RIS-assisted wireless systems outperform the corresponding AF-relaying ones in terms of average SNR, OP, SER and EC.

INDEX TERMS Amplify-and-forward, average signal-to-noise-ratio, beyond 5G systems, ergodic capacity, high-signal-to-noise-ratio approximation, meta-surfaces, multipath fading, outage probability, performance analysis, reconfigurable intelligent surfaces, symbol error rate, theoretical framework.

NOMENCLATURE

2D	Two dimensional
3D	Three dimensional
AF	Amplify-and-forward
AWGN	Additive white Gaussian noise
B5G	Beyond fifth generation
BER	Bit error rate
BPAM	Binary pulse amplitude modulation
BPPM	Binary pulse position modulation
BPSK	Binary phase shift keying
CDF	Cumulative density function
D	Destination
e2e	End-to-end
EC	Ergodic capacity
EM	Electromagnetic
KPM	Key performance metric
MISO	Multi-input single-output
MS	Metasurface
NOMA	Non-orthogonal multiple access
OP	Outage probability
PAM	Pulse amplitude modulation
PDF	Probability density function
PS	Phase shift
PSK	Phase shift keying
QAM	Quadrature amplitude modulation

The associate editor coordinating the review of this manuscript and approving it for publication was Prakasam Periasamy.

QPSK	Quadrature phase shift keying
R	Relay
RF	Radio frequency
RIS	Reconfigurable intelligent surface
RV	Random variable
S	Source
SER	Symbol error rate
SINR	Signal-to-interference-plus-noise-ratio
SNR	Signal-to-noise-ratio
ZMCG	Zero-mean complex Gaussian

I. INTRODUCTION

The evolution of the wireless world towards the beyond fifth generation (B5G) era comes with higher reliability, data-rates and traffic demands, which is driven by innovative applications, such as unmanned mobility, three dimensional (3D) media, augmented and virtual reality [1]–[4]. Technological advances, such as massive multiple-input multiple-output, full-duplexing, and millimeter-wave communications, have been advocated, due to their increased hardware cost, power consumption [5]–[7], as well as their need to operate in unfavorable electromagnetic (EM) wave propagation environment, where they have to deal with a number of medium particularities [8], [9].

As a remedy, the exploitation of the implicit randomness of the propagation environment through reconfigurable intelligent surfaces (RISs), in order to improve the quality of service and experience, attracts the eyes of both academia and industry [3], [10]–[12]. Most RIS implementations consist of two dimensional (2D) metasurface (MS) arrays, which are controlled by at least one microcontroller, and are capable of altering the incoming EM field in a customized manner [13]. In more detail, each MS can independently configure the phase shift (PS) of the EM signal incident upon it; hence, they are able to collaboratively create a preferable wireless channel [14]. In other words, RIS can amplify-and-forward (AF) the incoming signal without employing a power amplifier. Due to this functionality, the technological approach that can be considered equivalent and has the most similarity to RIS is AF-relaying [5], [15]–[17]. As a consequence, the question of whether RIS-assisted systems can outperforms AF-relaying ones and under which conditions arises.

A. RELATED WORK

Scanning the technical literature, a lot of research effort was put on the design, demonstration, optimization, and analysis of RIS and RIS-assisted wireless systems (see e.g., [5], [12], [14]–[16], [18]–[36] and references therein). For example, in [18], the authors introduced a RIS that consists of 102 MSs operates in 2.47 GHz, for indoor applications. Similarly, in [19], the authors reported a reconfigurable MS with adjustable polarization, scattering and focusing control, while, in [20], intelligent walls, which were equipped with frequency-selective MSs, were presented. Likewise, in [21], a MS capable of rotating a linear polarized EM wave by 90° was reported, whereas, in [22], an ultra-thin MS based on phase discontinuities was proposed to manipulate EM waves in the microwave band. Moreover, in [23], a RIS design that employed varactor-tuned resonators in order to enable tunable PS by adjusting the bias voltage applied to the varactor, was delivered, while, in [24] and [25], its functionality was demonstrated. Finally, in [26], RIS elements whose EM response were controlled by PIN diodes were reported.

From the optimization point of view, in [27], an asymptotic uplink ergodic data-rate investigation of RIS-assisted systems under Rician fading was performed, while, preliminary optimization frameworks for the maximization of the total received power in RIS-assisted wireless systems were reported in [14] and [28]. Specifically, in [14], the values of the PSs, which were created by the MSs, were optimized in a RIS-assisted single-user multiple-input-single-output (MISO) wireless system, whereas, in [28], the authors solved the same problem, in a more realistic scenario, in which the RIS consisted by a finite number of discrete PSs. Moreover, in [29], optimal linear precoder, power allocation and RIS phase matrix designs that used the large-scale statistics channel knowledge and aimed at maximizing the minimum signal-to-noise-plus-interference ratio (SINR) at the base-station were reported. Likewise, in [5] the problem of maximizing the weighted sum rate of all users through jointly optimizing the active precoding matrices at the base-stations and the PSs at RIS-assisted multi-user wireless networks is formulated and solved, while, in [16], the joint maximization of the sum-rate and the energy efficiency was investigated for a multi-user downlink scenario. Furthermore, in [30], the optimization problem of simultaneous wireless information and power transfer in RIS-assisted systems was studied. Meanwhile, in [32], a downlink multi-user scenario, in which a multi-antenna base-station, which is capable of performing digital beamforming, communicates with various users through a finite-size RIS was presented and an iterative algorithm was designed in order to maximize the sum rate.

From the theoretical analysis point of view, in [15] and [31], the authors provided a symbol error rate (SER) upper-bound for RIS-assisted wireless systems. It is worth noting that these upper-bounds are quite tight for RIS utilizations with high-number of MSs, but, for a low-number of MSs, they are not so accurate. Similarly, in [33], a bit error rate (BER) analysis was provided for RIS-assisted non-orthogonal multiple access (NOMA) systems. Again, the authors employed the central limit theorem in order to model the distribution of the equivalent base station-user equipment channel. As a consequence, the results are accurate only for scenarios in which the RIS consists of a large number of MSs. In [34], Jung et. al provided an asymptotic analysis of the uplink sum-rate of a RIS-assisted system, assuming that the established channels follow Rician distribution. Finally, in [35], Björnson et. al compared the performance of RIS-assisted systems against decode-and-forward relaying ones in terms of energy efficiency,

assuming deterministic channels, while, in [36], Renzo et. al revealed the key differences and similarities between RISs and relays. Also, in [36], simulations were used in order to compare RIS and relays in terms of data-rate.

On the other hand, there are several published contributions that investigate the performance of AF-relaying assisted wireless systems(see e.g., [37]–[50] and reference therein). In more detail, in [37], the authors reported closed-form expressions for the probability density function (PDF) and cumulative density function (CDF) of the end-to-end (e2e) signal-to-noise-ratio (SNR), assuming that the intermediate channels are Rayleigh distributed. Similarly, in [38] and in [39], tight-approximations for the system's SER were presented. Moreover,in [40] an asymptotic SER analysis of AF-relaying systems was conducted, while, in [41] and in [42], SER lower bounds were presented assuming that differential and frequency shift keying modulation schemes are respectively used. Furthermore, in [43], closed-form expressions for the outage probability (OP) of AF cognitive relay networks were presented accompanied by a lower bound SER expressions. Likewise, in [44], the authors reported closed-form expressions for the OP of switch-and-stay AF relay networks, whereas, in [45], OP approximations for selection AF relaying systems were presented. Moreover, in [46]–[49], the authors provided closed-form expressions for the OP and bounds for the ergodic capacity (EC) of a dual-hop variable-gain AF relaying system. Similarly, for the corresponding fixed-gain AF relaying system, in [50], the authors derived EC approximations. To sum up, the literature review revealed that, although a great amount of effort was put on analyzing the performance of AF relaying systems, no closed-form tractable expression for the average SNR and EC was reported. Finally, to the best of the authors knowledge, no generalized expression for the SER of such systems was presented.

B. MOTIVATION, NOVELTY AND CONTRIBUTION

Despite of the paramount importance that RIS-assisted wireless systems are expected to play in B5G setups, their performance has been only assessed in terms of SER lower-bounds. Likewise, to the best of the authors knowledge, regardless of their similarities with the AF-relaying systems, no analytical comparison between RIS-assisted and conventional AF-relaying wireless systems has been conducted. Motivated by this, this work focuses on presenting the theoretical framework that quantifies the performance of the RIS-assisted wireless system. Moreover, an analytic comparison between the aforementioned wireless systems, in terms of average SNR, OP, SER, and EC, is conducted. In more detail, the technical contribution of this paper is as follows:

- Novel analytical expressions for the PDF and CDF of e2e wireless fading channel coefficient of the RIS-assisted wireless system, are derived, which take into account the number of the RIS MSs and assume that the source (S)-RIS and RIS-destination (D) links experience Rayleigh fading. Notice that this is the first time that the aforementioned expressions are reported in the literature. Moreover, closed-form expressions for the PDF and the CDF of the e2e wireless fading channel for the special case, in which the RIS is equipped with only one MS, are also presented.
- Next, the instantaneous and average e2e SNR for the RIS-assisted wireless system are derived. Building upon them, the diversity gain of the RIS-assisted wireless system is extracted, as well as close-form expressions for the PDF and CDF of its e2e SNR. Furthermore, analytic expressions for the SNR statistical characterization, for the special case in which the RIS is equipped with only one MS, are provided. From these expressions, the diversity gain is analytically evaluated for both cases of single and multiple-MSs.
- To quantify the outage performance of the RIS-assisted wireless system, we derive low-complexity closed-form expressions for its OP for both cases, in which the RIS is equipped with multiple and single MS. These expressions reveal the relation between the number of MS, the transmission power and spectral efficiency with the system outage performance; hence, they provide useful insights and can be used as design tools.
- Closed-form expressions for the SER of a large variety of Gray-mapped modulation schemes for the RIS-assisted wireless systems are provided, for both cases in which the RIS consists of multiple and single MS. Furthermore, tight low-computational complexity approximations for the SER in the high-SNR regime are extracted.
- Building upon the high-SNR SER approximation, we derive a simple closed-form expression for the RIS-assisted wireless system diversity order, which highlights that the diversity order is a linear function of the number of MSs.
- Analytical expressions for the EC of the RIS-assisted wireless system for both cases, in which the RIS is equipped with multiple and a single MS, are also reported. Likewise, tight high-SNR and high-MS number approximations for the EC are derived. Moreover, an alternative more elegant EC expression, which is capable of providing interesting observations, is extracted.
- Finally, in order to compare the RIS-assisted wireless system with the corresponding AF-relaying one, we provide the analytical framework for the derivation of the average e2e SNR, OP, SER, and EC of the AF-relaying wireless system.Note that although the PDF and CDF of the e2e SNR of the AF-relaying wireless system has been initially presented in [37], to the best of the authors knowledge, this is the first time that closed-form expressions for the average e2e SNR, SER, and EC are reported in the technical literature. Finally, comparative results, which shows the superiority of the RIS-assisted system against the AF-relaying one, are presented.

It is worth-noting that, for the special case in which RIS is equipped with a single MS, the e2e equivalent channel follows a double Rayleigh distribution. This distribution has been extensively examined in the literature [51], [52]. As a result, the OP expressions that are presented in this paper for this special case have been previously reported in several published works, including [51], [53] under different frameworks. On the other hand, this is the first time that the generalized SER and EC expressions, which refer the single-MS RIS system, are presented in the literature.

C. ORGANIZATION AND NOTATIONS

The remainder of this work is organized as follows: Section II provides the RIS-assisted and AF-relaying wireless system models as well as the statistical characterization of the RIS-assisted e2e wireless channel. Next, Section III presents the performance analysis of both the RIS-assisted and AF-relaying wireless systems, while, Section IV reports respective numerical results and discussions. Finally, a summary of this work accompanied by closing remarks and key observations are provided in Section V.

NOTATIONS

The operators $\mathbb{E}[\cdot]$, $\mathbb{V}[\cdot]$ and $|\cdot|$ respectively denote the statistical expectation, variance, and the absolute value, whereas $\exp(x)$ and $\log_2(x)$ respectively stand for the exponential and the binary logarithmic functions. Additionally, $\ln(x)$ refers to the natural logarithm of x, while $\sqrt{x}$ and $\lim_{x\to a}(f(x))$ respectively return the square root of x and the limit of the function $f(x)$ as x tends to a. Furthermore, $\min(\mathcal{A})$ returns the minimum value of the set $\mathcal{A}$ and $(x)_n$ denotes the Pochhammer operator [54, eq. (19)]. Likewise, $\csc(x)$ and $\operatorname{acsc}(x)$ respectively give the cosecant and the arc cosecant of x, while $\sec(x)$ returns the secant of x [55, ch. 6]. The upper and lower incomplete Gamma functions [56, eq. (8.350/2), (8.350/3)] are respectively denoted by $\Gamma(\cdot,\cdot)$ and $\gamma(\cdot,\cdot)$, while the Gamma function is represented by $\Gamma(\cdot)$ [56, eq. (8.310)]. The E and error functions are respectively represented by $\mathrm{Q}3(\cdot)$ [57, ch. 2] and $\mathrm{erf}(\cdot)$ [58, eq. (7.1.1)], whereas $K_v(\cdot)$ and $I_v(\cdot)$ are respectively the modified Bessel function of the second [58, eq. (9.6.2)] and first kind of order v [58, eq. (9.6.3)]. Moreover, $F_0(\cdot)$, $\mathrm{E}(\cdot)$, and $\mathrm{K}(\cdot)$ respectively represent the polygamma function of the zero order [58, eq. (6.4.1)], the elliptic integral function [58, eq. (17.1.1)], and the complete elliptic integral function of the first kind [58, eq. (17.3.1)]. Furthermore, ${}_2F_1(\cdot,\cdot;\cdot;\cdot)$ stands for the Gauss hypergeometric function [58, eq. (4.1.1)], while ${}_pF_q\left(a_1,\cdots,a_p;b_1,\cdots,b_q;x\right)$ is the generalized hypergeometric function [56, eq. (9.14/1)]. Meanwhile, $U(a,b,x)$ and $G_{p,q}^{m,n}\left(x\left|\begin{matrix}a_1,a_2,\cdots,a_p\\b_1,b_2,\cdots,b_q\end{matrix}\right.\right)$ respectively represent the confluent hypergeometric function of second kind [56, ch. 9.2], and the Meijer's G-function [56, eq. (9.301)], whereas $H_{p,q}^{m,n}\left[z\left|\begin{matrix}(a_1,b_1),\cdots,(a_p,b_p)\\(c_1,d_1),\cdots,(c_p,d_p)\end{matrix}\right.\right]$ and $G_{p_1,p_2:p_3,q_1:q_2,q_3}^{m_1,m_2:m_3,n_1:n_2,n_3}\left(\begin{matrix}\cdot,\cdots,\cdot\\\cdot,\cdots,\cdot\end{matrix}\left|\begin{matrix}\cdot,\cdots,\cdot\\\cdot,\cdots,\cdot\end{matrix}\right|\begin{matrix}\cdot,\cdots,\cdot\\\cdot,\cdots,\cdot\end{matrix}\right|x,y\right)$ is the Fox H-function [59, eq. (8.3.1/1)] and the generalized Meijer G-function of two variables [60].

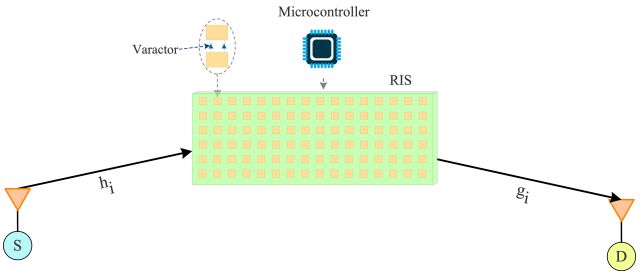

FIGURE 1. System model of the RIS-assisted wireless system.

II. SYSTEM MODEL

In this section, the system models of the RIS-assisted and AF-relaying wireless systems are provided. In more detail, in Section II-A, the RIS-assisted wireless system model is reported accompanied by the statistical characterization of its e2e wireless channel, while the system model of the corresponding AF-relaying setup is delivered in Section II-B.

A. RIS-ASSISTED WIRELESS SYSTEM

As depicted in Fig. 1, for the RIS-assisted wireless system, we consider a scenario, in which a single-antenna S node communicates with a single-antenna D node through a RIS, that consists of N MSs. The baseband equivalent fading channels between S and the i-th MS of the RIS, h_i, as well as the one between the $i-$th MS and D, g_i, are assumed to be independent, identical, slowing varying, flat, and their envelop follow Rayleigh distributions with scale parameters being equal to 1.[1] For clarity, we highlight that, as usual practice, the deterministic path-gain is not considered in the fading coefficients h_i and g_i.

The baseband equivalent received signal at D can be expressed as [15]

$$y = \sum_{i=1}^{N} h_i g_i r_i x + n, \tag{1}$$

where n denotes the additive white Gaussian noise (AWGN) and can be modeled as a zero-mean complex Gaussian (ZMCG) process with variance equal N_o. Additionally, r_i represents the i-th MS response and can be obtained as

$$r_i = |r_i| \exp(j\theta_i), \tag{2}$$

with θ_i being the PS applied by the $i-$th reflecting MS of the RIS. In this work, it is assumed that the reflected units of the RIS are equipped with varactor-tuned resonators that are able to achieve tunable PS by adjusting the bias voltage applied

[1] This assumption was used in several previously published works including [15], [16], [61], [62] and references therein. This assumption originates from the fact that even if the line-of-sight links between S-RIS and RIS-D are blocked, there still exist extensive scatters.

to the varactor [24]. Additionally, we assume that the phases of the channels h_i and g_i are perfectly known to the RIS, and that the RIS choices the optimal phase shifting, i.e.,

$$\theta_i = -\left(\phi_{h_i} + \phi_{g_i}\right), \tag{3}$$

where ϕ_{h_i} and ϕ_{g_i} are respectively the phases of h_i and g_i. Likewise, without loss of generality, it is assumed that the reflected gain of the $i-$th MS, $|g_i|$, is equal to 1. Notice that according to [63], this is a realistic assumption. Hence, (2) can be simplified as

$$r_i = \exp\left(-j\left(\phi_{h_i} + \phi_{g_i}\right)\right). \tag{4}$$

Additionally, by employing (4), (1) can be re-written as

$$y = Ax + n, \tag{5}$$

where A is the e2e baseband equivalent channel coefficient and can be obtained as

$$A = \sum_{i=1}^{N} |h_i||g_i|. \tag{6}$$

From (6), it is evident that the system experiences a diversity gain that depends on the number of MSs. Next, we provide the theoretical framework for the characterization of the e2e channel coefficient.

Statistical Characterization of the e2e Channel: The following theorem returns closed-form approximation for the PDF and CDF of A.

Theorem 1: The PDF and CDF of A can be respectively evaluated as

$$f_A(x) = \frac{x^a}{b^{a+1}\Gamma(a+1)} \exp\left(-\frac{x}{b}\right) \tag{7}$$

and

$$F_A(x) = \frac{\gamma\left(1+a, \frac{x}{b}\right)}{\Gamma\left(a+1\right)}, \tag{8}$$

where

$$a = \frac{k_1^2}{k_2} - 1, \tag{9}$$

and

$$b = \frac{k_2}{k_1}, \tag{10}$$

with

$$k_1 = \frac{N\pi}{2}, \tag{11}$$

and

$$k_2 = 4N\left(1 - \frac{\pi^2}{16}\right). \tag{12}$$

Proof: Please refer to Appendix A. ■

Special Case: For the special case in which the RIS consists of a single MS, i.e. $N = 1$, A is the product of two independent and identical Rayleigh distributed random variables (RVs); thus, it follows a double Rayleigh distribution and its PDF and CDF can be respectively obtained as [51, eqs. (3), (4)]

$$f_A^s = xK_0\left(x\right) \tag{13}$$

and

$$F_A^s = 1 - xK_1\left(x\right), \tag{14}$$

where $K_0(x)$ and $K_1(x)$ represent the modified Bessel functions of the second kind of order 0 and 1, respectively.

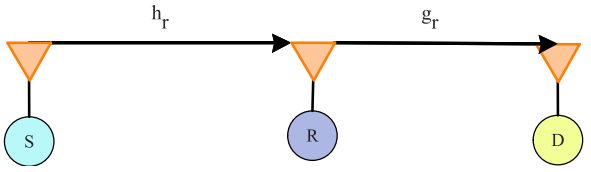

FIGURE 2. System model of the AF relay-assisted wireless system.

B. AF-RELAYING WIRELESS SYSTEM

The block diagram of the AF-relaying wireless system is illustrated in Fig. 2. In this setup, we consider that that S communicates with D through an AF relay (R) node. All the involved nodes are equipped with a single radio frequency (RF) chain that feeds a single-antenna. By assuming that the transmitted by S data symbol, x conveys through a flat fading channel h_r, the received signal at R can be obtained as

$$y_r = h_r x + n_r, \tag{15}$$

where $|h_r|$ is modeled as a Rayleigh process with scale parameter equals 1. Likewise, n_r is a ZMCG process with variance N_o and stands for the AWGN at R.

According to the AF-relaying protocol, R amplifies the received signal and re-transmit it to D. Thus, the baseband equivalent received signal at D can be expressed as

$$y_d = g_r G y_r + n_d, \tag{16}$$

or equivalently

$$y_d = \sqrt{G} g_r h_r x + G n_r + n_d, \tag{17}$$

where G, g_r and n_d are independent and respectively stand for the R amplification gain, the R-D channel coefficient, and the AWGN at D. Of note, $|g_r|$ and n_d are respectively modeled as a Rayleigh process with scale parameter 1 and zero-mean complex Gaussian process with variance equals N_o. For the sake of fairness, we assume that the relay have perfect knowledge of both the h_r and g_r [64]–[66].

III. PERFORMANCE ANALYSIS

This section focuses on presenting the theoretical framework for the performance analysis of both the RIS-assisted and AF-relaying wireless systems. In particular, Section III-A is devoted to the extraction of the key performance metrics (KPMs) for RIS-assisted wireless systems, whereas the KPMs for the AF relaying wireless system are reported in

Section III-B. The expressions that are presented here provides insightful remarks and are expected to be used in the design of RIS-assisted systems as well as their comparison against corresponding AF-relaying ones.

A. RIS-ASSISTED WIRELESS SYSTEMS

The organization of this section is as follows: Section III-A1 presents closed-form expressions for the instantaneous and average e2e SNR as well as its statistical characterization. Based on these expressions, the theoretical framework for the system outage performance is provided in Section III-A2, while analytical expressions for the evaluation of the SER are reported in Section III-A3. Finally, Sections III-A4 and III-A5 respectively deliver the analytical framework for the evaluation of the diversity order and EC.

1) SNR

According to (5), the instantaneous e2e SNR of the RIS-assisted wireless system can be obtained as

$$\rho = A^2 \rho_s, \tag{18}$$

where

$$\rho_s = \frac{E_s}{N_o}, \tag{19}$$

with E_s being the S transmitted power.

Theorem 2 returns a closed-form expression for the average e2e SNR, while Theorem 3 delivers closed-form expressions for its PDF and CDF.

Theorem 2: The average e2e SNR can be obtained as

$$\mathbb{E}[\rho] = \frac{\Gamma(a+3)b^2}{\Gamma(a+1)}\rho_s. \tag{20}$$

Proof: Please refer to Appendix B. ■

From (20), it is evident that the diversity gain of the RIS-assisted wireless system can be evaluated as

$$G_{\text{RIS}} = \frac{\Gamma(a+3)b^2}{\Gamma(a+1)}, \tag{21}$$

or equivalently,

$$G_{\text{RIS}} = (a+1)_2\, b^2, \tag{22}$$

which by employing (9)–(12) can be rewritten as

$$G_{\text{RIS}} = \left(\frac{16-\pi^2}{2\pi}\right)^2 \left(\frac{\pi^2}{16-\pi^2}N\right)_2. \tag{23}$$

Interestingly, (23) reveals that the only way to increase the diversity gain of the RIS-assisted wireless system is to increase the number of MSs in the RIS.

Next, we characterize the statistics of the e2e SNR. In this direction, Theorem 3 provides novel closed-form expressions for its PDF and CDF.

Theorem 3: The PDF and the CDF of the e2e SNR can be respectively evaluated as

$$f_\rho(x) = \frac{1}{2b^{a+1}\Gamma(a+1)\,\rho_s^{\frac{a+1}{2}}} x^{\frac{a-1}{2}} \exp\left(-\frac{1}{b}\sqrt{\frac{x}{\rho_s}}\right) \tag{24}$$

and

$$F_\rho(x) = \frac{\gamma\left(a+1, \frac{1}{b}\sqrt{\frac{x}{\rho_s}}\right)}{\Gamma(a+1)}. \tag{25}$$

Proof: Please refer to Appendix C. ■

Special Case: For the special case in which $N = 1$, the following lemmas return closed-form expressions for the PDF, CDF and average equivalent e2e SNR.

Lemma 1: For $N = 1$, the CDF and PDF of the equivalent e2e SNR can be respectively obtained as

$$F_\rho^s(x) = 1 - \sqrt{\frac{x}{\rho_s}} K_1\left(\sqrt{\frac{x}{\rho_s}}\right) \tag{26}$$

and

$$f_\rho^s(x) = \frac{1}{4\rho_s} K_0\left(\sqrt{\frac{x}{\rho_s}}\right) - \frac{1}{2\sqrt{\rho_s x}} K_1\left(\sqrt{\frac{x}{\rho_s}}\right) + \frac{1}{4\rho_s} K_2\left(\sqrt{\frac{x}{\rho_s}}\right). \tag{27}$$

Proof: Please refer to Appendix D. ■

Lemma 2: For $N = 1$, the average equivalent e2e SNR can be obtained as

$$\mathbb{E}\left[\rho^s\right] = 4\rho_s. \tag{28}$$

Proof: Please refer to Appendix E. ■

From (28), it becomes evident that the diversity gain of the single-MS RIS-assisted wireless system is equal to 4.

2) OUTAGE PROBABILITY

The OP is defined as the probability that the e2e instantaneous SNR falls below a predetermined threshold, ρ_{th}, i.e.

$$P_o = P_r\left(\rho \le \rho_{th}\right), \tag{29}$$

or equivalently

$$P_o = F_\rho\left(\rho_{th}\right), \tag{30}$$

which, by employing (25), can be written as

$$P_o = \frac{\gamma\left(a+1, \frac{1}{b}\sqrt{\frac{\rho_{th}}{\rho_s}}\right)}{\Gamma(a+1)}. \tag{31}$$

Moreover, by employing (9)–(12), (31) can be rewritten as

$$P_o = \frac{\gamma\left(\frac{\pi^2}{16-\pi^2}N, \frac{2\pi}{16-\pi^2}\sqrt{\frac{\rho_{th}}{\rho_s}}\right)}{\Gamma\left(\frac{\pi^2}{16-\pi^2}N\right)}. \tag{32}$$

From (32), we observe that, for a fixed $\frac{\rho_{th}}{\rho_s}$, as N increases, the OP decreases; thus, the outage performance improves. Similarly, for a given N, as $\frac{\rho_{th}}{\rho_s}$ increases, the OP decreases.

Special Case: For the special case in which $N = 1$, the OP can be obtained as

$$P_o^s = F_\rho^s\left(\rho_{th}\right), \tag{33}$$

or, by using (26), as

$$P_o^s = 1 - \sqrt{\frac{\rho_{th}}{\rho_s}} K_1\left(\sqrt{\frac{\rho_{th}}{\rho_s}}\right). \tag{34}$$

From (34), it is observed that in the special case in which $N = 1$, the outage performance of the RIS-assisted wireless system depend only from $\frac{\rho_{th}}{\rho_s}$, i.e., the transmitted signal characteristics, namely spectral efficiency and transmission power. In more detail, as the spectral efficiency of the transmission scheme increases, ρ_t also increases; thus, $\frac{\rho_{th}}{\rho_s}$ increases and an outage performance degradation is observed. On the other hand, as the transmission power increases, $\frac{\rho_{th}}{\rho_s}$ decreases; therefore, the OP also decreases.

3) SER

The following theorem returns a closed-form expression for the SER of the RIS-assisted wireless system.

Theorem 4: The SER can be analytically evaluated as in (35)*, as shown at the bottom of the next page.*

Proof: Please refer to Appendix F. ∎

In (35), c and d are modulation specific constants. For example, the SER of binary phase shift keying (BPSK) can be obtained for $c = d = 1$, while for M pulse-amplitude modulation (M-PAM) for $c = \frac{2(M-1)}{M}$ and $d = \frac{3}{M^2-1}$. Likewise, for $c = 1$ and $d = 0.5$, we can obtain the SER for the case in which binary pulse position modulation (BPPM) is employed, whereas, for $c = 2$ and $d = 1$, the one of quadrature phase shift keying (QPSK) can be evaluated. Finally, for $c = 2$ and $d = \sin^2\left(\frac{\pi}{M}\right)$, the SER of M-phase shift keying (M-PSK) can be obtained, while, for $c = 4\left(1 - \frac{1}{\sqrt{M}}\right)$ and $d = \frac{3}{2}\frac{1}{M-1}$, (35) returns the SER of M-quadrature amplitude modulation (M-QAM) with $M > 4$.

The following corollary provides a high-SNR approximation of the SER.

Corollary 1: In the high-SNR regime, the SER can be approximated as in (36)*, as shown at the bottom of the next page.*

Proof: In the high-SNR regime, i.e., for $\rho_s \to \infty$, the following expressions holds:

$$\lim_{y\to 0} {}_2F_4\left(\frac{a+1}{4}, \frac{a+3}{4}; \frac{1}{4}, \frac{1}{2}, \frac{3}{4}, \frac{a+5}{4}; y\right) = 1, \quad (37)$$

$$\lim_{y\to 0} {}_2F_4\left(\frac{a+2}{4}, \frac{a+4}{4}; \frac{1}{2}, \frac{3}{4}, \frac{5}{4}, \frac{a+6}{4}; y\right) = 1, \quad (38)$$

$$\lim_{y\to 0} {}_2F_4\left(\frac{a+3}{4}, \frac{a+5}{4}; \frac{3}{4}, \frac{5}{4}, \frac{3}{2}, \frac{a+7}{4}; y\right) = 1 \quad (39)$$

and

$$\lim_{y\to 0} {}_2F_4\left(\frac{a+4}{4}, \frac{a+6}{4}; \frac{5}{4}, \frac{3}{2}, \frac{7}{4}, y\right) = 1, \quad (40)$$

where

$$y = \frac{1}{256 b^4 d^2 \rho_s^2}. \quad (41)$$

Hence, by substituting (37)-(40), we obtain (36). This concludes the proof. ∎

From (36), we observe that the first term of the sum is the dominant one. This observation leads to the following remark: the SER is a decreasing function of ρ_s and a, and an increasing function of c. This indicates that as the transmission power increases and/or the number of MS increases, the SER decreases, while as modulation order increases, the error performance degrades.

Special Case: For the special case in which $N = 1$, the following lemma returns a closed-form expression for the SER.

Lemma 3: For $N = 1$, the SER can be analytically computed as

$$P_e^s = \frac{\sqrt{\pi}}{4}\frac{c}{2}\mathrm{U}\left(\frac{1}{2}, 0, \frac{1}{4d\rho_s}\right) - 1. \quad (42)$$

Proof: Please refer to Appendix G. ∎

According to (42), in the special case in which $N = 1$, the SER increases, as the modulation order increases, while, as ρ_s increases, the SER decreases.

4) DIVERSITY ORDER

Theorem 5 returns the diversity order of the RIS-assisted wireless system.

Theorem 5: The diversity order of the RIS-assisted wireless system can be calculated as

$$D = \frac{N}{2}\frac{\pi^2}{16 - \pi^2}. \quad (43)$$

Proof: Please refer to Appendix H. ∎

Based on (43), the diversity order is a linearly increasing function of N. Note that in the same conclusion was extracted in [15] and [31].

5) ERGODIC CAPACITY

The following theorems return two equivalent and novel closed-form expressions for the EC.

Theorem 6: The EC of the RIS-assisted wireless system can be analytically computed as in (44)*, as shown at the bottom of the next page.*

Proof: Please refer to Appendix I. ∎

Theorem 7: The EC of the RIS-assisted wireless system can be alternatively evaluated as in (45)*, as shown at the bottom of the next page.*

Proof: Please refer to Appendix J. ∎

Notice that (44) returns the EC as a sum of well-defined special functions that can be directly evaluated in several software packages, such as Mathematica, Mapple, Matlab, etc. However, it is quite difficult or even impossible to obtain insightful observations from this expression. On the other hand, a more elegant expression for the EC is presented in (45), which can be evaluated directly in Mathematica, by rewritten the Fox H function as a generalized Meijer's G-function. Moreover, from (45), it is revealed that the EC is an increasing function of ρ_s and N.

The following corollaries present high-SNR and high-N approximations for the EC.

Corollary 2: In the high SNR regime, the EC can be approximated as in (46)*, as shown at the bottom of the next page.*

Proof: For $\rho_s \to \infty$, $y = -\frac{1}{4\,b^2\rho_s} \to 0$. Moreover,

$$\lim_{y\to 0} {}_1F_2\left(1+\frac{a}{2}; \frac{3}{2}, 2+\frac{a}{2}, -y\right) = 1, \tag{47}$$

$$\lim_{y\to 0} {}_1F_2\left(\frac{a+1}{2}; \frac{1}{2}, \frac{a+3}{2}, -y\right) = 1 \tag{48}$$

and

$$\lim_{y\to 0} {}_2F_3\left(1, 1; 2, 1-\frac{a}{2}, \frac{3-a}{2}, -y\right) = 1. \tag{49}$$

Thus,in the high SNR regime (44) can be approximated as in (46). This concludes the proof. ■

Corollary 3: In the high SNR and N regime, the EC can be approximated as

$$C_{\rho,N} \approx \frac{1}{\ln(2)(a-1)_2 b^2\rho_s} + \frac{a^2-a}{(a-1)_2}\log_2\left(b^2\rho_s\right) + \frac{2\left(a^2-a\right)}{\ln(2)(a-1)_2}F_0\left(3+a\right). \tag{50}$$

Proof: In the high SNR regime, as $N \to \infty$, $a \to \infty$; hence, since $\Gamma(a+1)$ is an increasing function, as $N \to \infty$, $\Gamma(a+1) \to \infty$, or equivalently $\frac{1}{\Gamma(a+1)} \to 0$. This indicates that the terms

$$\mathcal{A}_1 = \frac{\pi}{\ln(2)(2+a)b^{a+2}\Gamma(a+1)\rho_s^{\frac{a}{2}+1}}\csc\left(\frac{a\pi}{2}\right) \tag{51}$$

$$P_e = \frac{c}{2\sqrt{\pi}(a+1)b^{a+1}d^{\frac{a+1}{2}}\rho_s^{\frac{a+1}{2}}}\frac{\Gamma\left(\frac{a+3}{4}\right)}{\Gamma(a+1)}{}_2F_4\left(\frac{a+1}{4}, \frac{a+3}{4}; \frac{1}{4}, \frac{1}{2}, \frac{3}{4}, \frac{a+5}{4}; \frac{1}{256b^4d^2\rho_s^2}\right)$$
$$- \frac{c}{2\sqrt{\pi}(a+2)b^{a+2}d^{\frac{a+2}{2}}\rho_s^{\frac{a+2}{2}}}\frac{\Gamma\left(\frac{a+4}{4}\right)}{\Gamma(a+1)}{}_2F_4\left(\frac{a+2}{4}, \frac{a+4}{4}; \frac{1}{2}, \frac{3}{4}, \frac{5}{4}, \frac{a+6}{4}; \frac{1}{256b^4d^2\rho_s^2}\right)$$
$$+ \frac{c}{4\sqrt{\pi}(a+3)b^{a+3}d^{\frac{a+3}{2}}\rho_s^{\frac{a+3}{2}}}\frac{\Gamma\left(\frac{a+5}{4}\right)}{\Gamma(a+1)}{}_2F_4\left(\frac{a+3}{4}, \frac{a+5}{4}; \frac{3}{4}, \frac{5}{4}, \frac{3}{2}, \frac{a+7}{4}; \frac{1}{256b^4d^2\rho_s^2}\right)$$
$$- \frac{c}{12\sqrt{\pi}(a+4)b^{a+4}d^{\frac{a+4}{2}}\rho_s^{\frac{a+4}{2}}}\frac{\Gamma\left(\frac{a+5}{4}\right)}{\Gamma(a+1)}{}_2F_4\left(\frac{a+4}{4}, \frac{a+6}{4}; \frac{5}{4}, \frac{3}{2}, \frac{7}{4}, \frac{a+8}{4}; \frac{1}{256b^4d^2\rho_s^2}\right) \tag{35}$$

$$P_{e,s} \approx \frac{c}{2\sqrt{\pi}(a+1)b^{a+1}d^{\frac{a+1}{2}}\frac{\Gamma\left(\frac{a+3}{4}\right)}{\Gamma(a+1)}}\rho_s^{-\frac{a+1}{2}} - \frac{c}{2\sqrt{\pi}(a+2)b^{a+2}d^{\frac{a+2}{2}}}\frac{\Gamma\left(\frac{a+4}{4}\right)}{\Gamma(a+1)}\rho_s^{-\frac{a+2}{2}}$$
$$+ \frac{c}{4\sqrt{\pi}(a+3)b^{a+3}d^{\frac{a+3}{2}}\frac{\Gamma\left(\frac{a+5}{4}\right)}{\Gamma(a+1)}}\rho_s^{-\frac{a+3}{2}} - \frac{c}{12\sqrt{\pi}(a+4)b^{a+4}d^{\frac{a+4}{2}}}\frac{\Gamma\left(\frac{a+5}{4}\right)}{\Gamma(a+1)}\rho_s^{-\frac{a+4}{2}} \tag{36}$$

$$C = \frac{a^2-a}{(a-1)_2}\log_2\left(b^2\rho_s\right) + \frac{2\left(a^2-a\right)}{\ln(2)(a-1)_2}F_0\left(3+a\right)$$
$$+ \frac{\pi}{\ln(2)(2+a)b^{a+2}\Gamma(a+1)\rho_s^{\frac{a}{2}+1}}\csc\left(\frac{a\pi}{2}\right){}_1F_2\left(1+\frac{a}{2}; \frac{3}{2}, 2+\frac{a}{2}, -\frac{1}{4\,b^2\rho_s}\right)$$
$$+ \frac{\pi}{(a+1)b^{a+1}\ln(2)\,\Gamma(a+1)\rho_s^{\frac{a+1}{2}}}\sec\left(\frac{a\pi}{2}\right){}_1F_2\left(\frac{a+1}{2}; \frac{1}{2}, \frac{a+3}{2}, -\frac{1}{4b^2\rho_s}\right)$$
$$+ \frac{1}{\ln(2)(a-1)_2 b^2\rho_s}{}_2F_3\left(1, 1; 2, 1-\frac{a}{2}, \frac{3-a}{2}, -\frac{1}{4b^2\rho_s}\right) \tag{44}$$

$$C = 2\ln(2)\,b^2\Gamma(a+1)\rho_s H_{4,3}^{1,4}\left[b^2\rho_s\,\middle|\,\begin{matrix}(0,1),(0,1),(-a-2,2),(-a-3,2)\\(0,1),(-a-3,2),(-1,1)\end{matrix}\right] \tag{45}$$

$$C_\rho \approx \frac{1}{\ln(2)(a-1)_2\,b^2\rho_s} + \frac{a^2-a}{(a-1)_2}\log_2\left(b^2\rho_s\right) + \frac{2\left(a^2-a\right)}{\ln(2)(a-1)_2}F_0\left(3+a\right)$$
$$+ \frac{\pi}{\ln(2)(2+a)b^{a+2}\Gamma(a+1)\rho_s^{\frac{a}{2}+1}}\csc\left(\frac{a\pi}{2}\right) + \frac{\pi}{(a+1)b^{a+1}\ln(2)\,\Gamma(a+1)\rho_s^{\frac{a+1}{2}}}\sec\left(\frac{a\pi}{2}\right) \tag{46}$$

and

$$\mathcal{A}_2 = \frac{\pi}{(a+1)b^{a+1}\ln(2)\,\Gamma(a+1)\rho_s^{\frac{a+1}{2}}}\sec\left(\frac{a\pi}{2}\right) \quad (52)$$

tents to 0. Thus, (46) can be approximated as in (50). This concludes the proof. ∎

Special Case: In the special case in which $N = 1$, the following lemma returns a closed-form expression for the EC.

Lemma 4: For $N = 1$, the EC can be obtained as

$$C_s = \frac{1}{8\ln(2)\rho_s^2}G_{1,3}^{3,1}\left(\frac{1}{4\rho_s^2}\middle|\begin{matrix}-1\\-1,-1,0\end{matrix}\right) - \frac{1}{4\ln(2)\rho_s}G_{1,3}^{3,1}\left(\frac{1}{4\rho_s^2}\middle|\begin{matrix}-\frac{1}{2}\\-\frac{1}{2},-\frac{1}{2},-\frac{1}{2}\end{matrix}\right) + \frac{1}{8\ln(2)\rho_s^2}G_{2,4}^{4,1}\left(\frac{1}{4\rho_s^2}\middle|\begin{matrix}-1,0\\-1,-1,-1,1\end{matrix}\right). \quad (53)$$

Proof: Please refer to Appendix K. ∎

B. AF-RELAYING WIRELESS SYSTEMS

In this section, we revisit the theoretical framework of the AF-relaying wireless systems and, after defining their instantaneous SNR and presenting its PDF and CDF, we extract closed-form expressions for their average SNR, OP, SER and EC.

1) SNR

In the AF-relaying wireless system, based on (17) and by assuming variable amplification, the e2e instantaneous SNR can be obtained as [67, Eq. (2.144)]

$$\rho_r = \frac{\rho_1\rho_2}{\rho_1+\rho_2+1}, \quad (54)$$

or approximately

$$\rho_r \approx \frac{\rho_1\rho_2}{\rho_1+\rho_2}, \quad (55)$$

where

$$\rho_1 = |h_r|^2\rho_s \quad (56)$$

and

$$\rho_2 = |g_r|^2\rho_R, \quad (57)$$

with

$$\rho_R = \frac{E_r}{N_o} \quad (58)$$

and E_r denoting the R transmitted power.

The PDF and the CDF of ρ_r can be respectively written as [37, eqs. (19) and (27)]

$$f_{\rho_r}(x) = \frac{2}{\overline{\rho}_s\overline{\rho}_R}x\exp\left(-\left(\frac{1}{\overline{\rho}_s}+\frac{1}{\overline{\rho}_R}\right)x\right) \times\left(\frac{\overline{\rho}_s+\overline{\rho}_R}{\sqrt{\overline{\rho}_s\overline{\rho}_R}}K_1\left(\frac{2x}{\sqrt{\overline{\rho}_s\overline{\rho}_R}}\right)+2K_0\left(\frac{2x}{\sqrt{\overline{\rho}_s\overline{\rho}_R}}\right)\right) \quad (59)$$

and

$$F_{\rho_r}(x) = 1-\frac{2x}{\sqrt{\overline{\rho}_s\overline{\rho}_R}}\exp\left(-\left(\frac{1}{\overline{\rho}_s}+\frac{1}{\overline{\rho}_R}\right)x\right) \times K_1\left(\frac{2x}{\sqrt{\overline{\rho}_s\overline{\rho}_R}}\right), \quad (60)$$

where $\overline{\rho}_s$ and $\overline{\rho}_R$ are respectively the average SNR of the first and second hop and, since $|h_r|$ and $|g_r|$ are Rayleigh distributed processes with scale parameters equal 1, they can be respectively obtained as

$$\overline{\rho}_s = 2\rho_s \quad (61)$$

and

$$\overline{\rho}_R = 2\rho_R. \quad (62)$$

The following lemma provides a closed-form expression for the average e2e SNR of the AF-relaying wireless system.

Lemma 5: The average e2e SNR of the AF-relaying wireless system can be analytically evaluated as

$$\mathbb{E}[\rho_r] = -\frac{\beta^5+\beta^3\gamma^2-2\beta\gamma^4}{\left(-\beta^2+\gamma^2\right)^3}-\frac{\pi}{2}\frac{\beta^2\gamma^2-\gamma^4}{\left(-\beta^2+\gamma^2\right)^{5/2}} - \frac{3\beta\gamma^2}{\left(-\beta^2+\gamma^2\right)^2}+\frac{3\beta^2\gamma^2-2\beta\gamma^2}{\left(-\beta^2+\gamma^2\right)^{5/2}}\operatorname{arcsec}\left(\frac{\gamma}{\beta}\right), \quad (63)$$

for $\beta \neq \gamma$, and

$$\mathbb{E}[\rho_r] = \frac{2}{3\gamma}. \quad (64)$$

for $\beta = \gamma$, where

$$\beta = \frac{1}{\overline{\rho}_s}+\frac{1}{\overline{\rho}_R} \quad (65)$$

and

$$\gamma = \frac{2}{\sqrt{\overline{\rho}_s\overline{\rho}_R}}. \quad (66)$$

Proof: Please refer to Appendix L. ∎

Notice that $\beta = \gamma$ corresponds to $\overline{\rho}_s = \overline{\rho}_R$.

2) OUTAGE PROBABILITY

Similarly to Section III-A2, the OP of the AF-relaying wireless system can be obtained as

$$P_o^{\mathrm{AF}} = F_{\rho_r}(\rho_{th}). \quad (67)$$

3) SER

The following lemma delivers a closed-form expression for SER of AF-wireless systems.

Lemma 6: In AF-relaying wireless systems, the SER can be analytically evaluated as

$$P_e^{AF} = \frac{\sqrt{\gamma}c}{2}\sqrt{\frac{d}{2}}\frac{\beta+\gamma}{\gamma^2-(\beta+d)^2}\mathrm{E}\left(\frac{1}{2}-\frac{\beta+\gamma}{2\gamma}\right) - \frac{\sqrt{\gamma}c}{4}\sqrt{\frac{d}{2}}\frac{\beta+\gamma+d}{\gamma^2-(\beta+d)^2}\mathrm{K}\left(\frac{1}{2}-\frac{\beta+\gamma}{2\gamma}\right)-1. \quad (68)$$

Proof: Please refer to Appendix M. ∎

4) ERGODIC CAPACITY

The following lemma provides a closed-form expression for the EC of the AF-relaying wireless system.

Lemma 7: In AF-relaying wireless systems, the EC can be obtained as in (69), as shown at the bottom of the next page.

Proof: Please refer to Appendix N. ∎

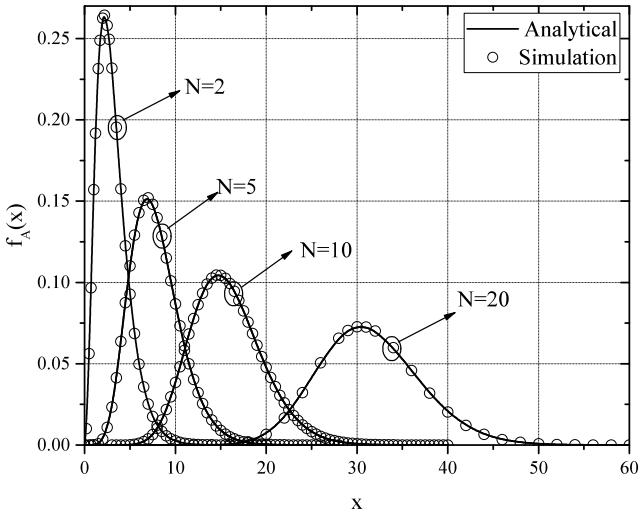

FIGURE 3. The PDF of the equivalent e2e channel for different N.

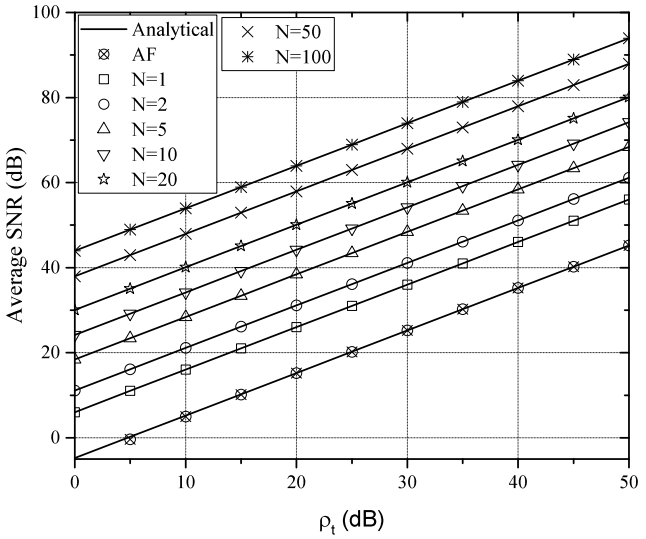

FIGURE 4. Average SNR vs ρ_t, for different N.

IV. RESULTS & DISCUSSION

This section is focused on verifying the theoretical framework through respective Monte Carlo simulations and reporting the RIS-assisted wireless system performance in comparison with the ones of the corresponding AF-relaying wireless system, in terms of e2e SNR, OP, SER and EC. Of note, for the sake of fair comparison, in the following results, we assume that the total transmission power of both the RIS-assisted and the AF-relaying wireless systems is the same. In other words, it is assumed that half of the S transmitted power in the RIS-assisted system is used for the S-R transmission and the other half for the R-D one in the AF-relaying wireless system. Finally, unless otherwise stated, in what follows, we use continuous lines and markers to respectively denote theoretical and simulation results.

Figure 3 illustrates the PDF of the equivalent e2e channel of the RIS-assisted wireless system, for different number of MSs, N. From this figure, it becomes evident that the analytical and simulation results coincide; thus, verifying the presented theoretical framework. Additionally, it is observed that, as N increases, the equivalent e2e channel values also increases. This indicates that by increasing N, we can improve the diversity gain of the RIS-assisted wireless system.

Figure 4 depicts the average e2e SNR of both the RIS-assisted and AF-relaying wireless systems as a function of ρ_t, for different values of N. Note that ρ_t represents the total transmission power to noise ratio. In other words, in the RIS-assisted wireless system, $\rho_t = \rho_s$, while in the AF-relaying wireless system $\rho_t = \rho_s + \rho_R$. From this figure, for the RIS-assisted system, we observe that, as theoretically proven in (20) and (28), for a given N, as ρ_t increases, the average e2e SNR linearly increases. The same applies for the AF-relaying system. Additionally, we observe that, for a given ρ_t, as N increases, the average e2e SNR improves. In more detail, for double values of N, the average e2e SNR increases by about 6 dB. Finally, it is evident that the RIS-assisted system outperforms the corresponding AF-relaying one, in terms of e2e average SNR, for all the values of N. Moreover, notice that even for $N = 1$, the RIS-assisted system achieves about 10 dB higher average e2e SNR compared to the AF-relaying system. This is due to the fact that the AF-relay, except from the AWGN at D, experiences an amplified additional noise, which is generated in R, while the RIS-assisted wireless system only experience the AWGN at D.

In Fig. 5, the outage performance of the RIS-assisted wireless system is quantified. In more detail, the OP is plotted as a function of $\frac{\rho_t}{\rho_{th}}$. As a benchmark, the OP of the AF-relaying wireless system is provided. As expected, in the RIS-assisted system, for a fixed N, as $\frac{\rho_t}{\rho_{th}}$ increases, the OP decreases.

$$C^{\mathrm{AF}} = \begin{cases} \frac{\sqrt{\pi}}{\ln(2)} \frac{\gamma^2}{(\beta-\gamma)^3} G_{2,1:2,2:1,2}^{0,2:1,2:2,0} \left(\begin{matrix} -2,-3 \\ -3 \end{matrix} \middle| \begin{matrix} 0,0 \\ 0,-1 \end{matrix} \middle| \begin{matrix} \frac{1}{2} \\ 0,0 \end{matrix} \middle| \begin{matrix} \frac{1}{\beta-\gamma}, \frac{2\gamma}{\beta-\gamma} \end{matrix} \right) \\ + \frac{\sqrt{\pi}}{\ln(2)} \frac{\beta\gamma}{(\beta-\gamma)^3} G_{2,1:2,2:1,2}^{0,2:1,2:2,0} \left(\begin{matrix} -2,-3 \\ -3 \end{matrix} \middle| \begin{matrix} 0,0 \\ 0,-1 \end{matrix} \middle| \begin{matrix} \frac{1}{2} \\ -1,-1 \end{matrix} \middle| \begin{matrix} \frac{1}{\beta-\gamma}, \frac{2\gamma}{\beta-\gamma} \end{matrix} \right), & \text{for } \beta \neq \gamma \\ \frac{\sqrt{\pi}}{\ln(2)} \gamma^2 \left(G_{3,4}^{4,1} \left(2\gamma \middle| \begin{matrix} -2,-1,\frac{1}{2} \\ 0,0,-2,-2 \end{matrix} \right) + G_{3,4}^{4,1} \left(2\gamma \middle| \begin{matrix} -2,-1,\frac{1}{2} \\ -1,1,-2,-2 \end{matrix} \right) \right), & \text{for } \beta = \gamma \end{cases} \quad (69)$$

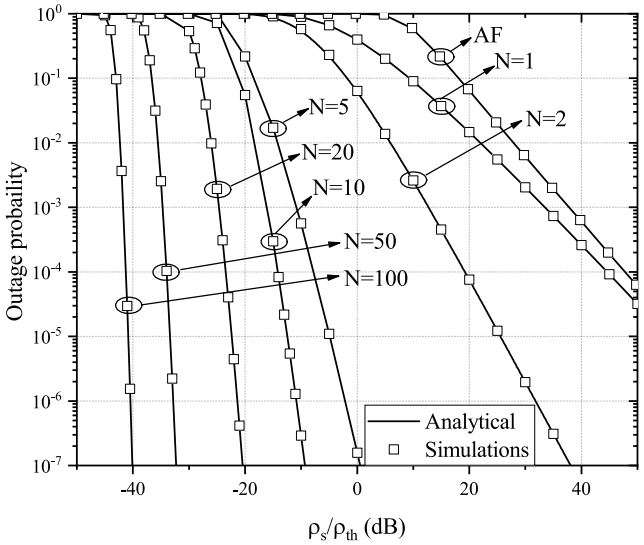

FIGURE 5. Outage probability vs $\frac{\rho_t}{\rho_{th}}$, for different values of N.

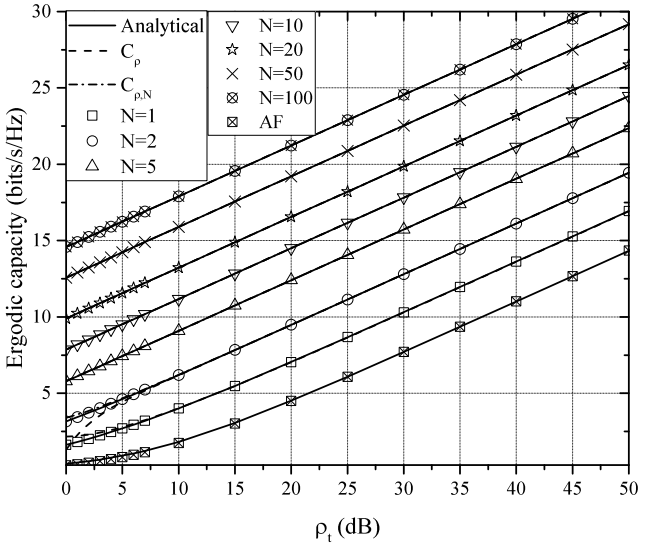

FIGURE 7. Capacity vs ρ_t, for different values of N.

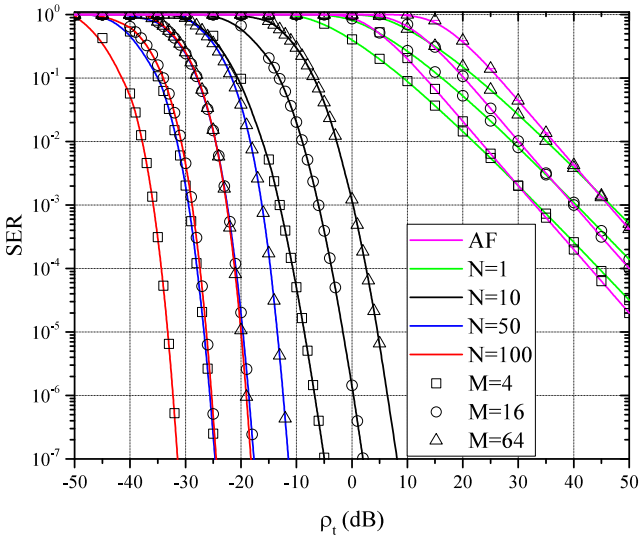

FIGURE 6. SER vs ρ_t, for different values of N and M, assuming $M-$QAM.

For example, for $N = 2$, as $\frac{\rho_t}{\rho_{th}}$ changes from 20 to 25 dB, the OP decreases approximately 10 times. Additionally, for a given $\frac{\rho_t}{\rho_{th}}$, as N increases, the outage performance improves. This indicates that for a given OP requirement, we can improve the RIS-assisted wireless system energy efficiency by increasing N. For instance, $\frac{\rho_t}{\rho_{th}}$ can be reduced by about 30 dB, by employing a RIS that consists of 5 MSs instead of one that consists of 2 in order to achieve an OP of 10^{-5}. Finally, it becomes evident that, the RIS-assisted wireless system outperforms the corresponding AF-relaying ones, in terms of OP.

In Fig. 6, the error performance of the RIS-assisted system as a function of ρ_t, for different $M-$QAM schemes and N, is demonstrated. As a benchmark, the SER of the corresponding AF-relaying systems is also plotted. As expected, for a given N and M, as ρ_t increases, the SER performance improves. For example, for $N = 10$ and $M = 16$, as ρ_t shifts from -4 to 0 dB, the SER decreases by about 100 times. Moreover, we observe that, for fixed M and a SER requirement, as N increases, the ρ_t gain is significantly enhanced. For instance, for $M = 16$ and SER requirement set to 10^{-4}, a 52 dB transmission SNR gain is observed as N increases from 1 to 10. Additionally, for given N and SER requirement, as M increases, a ρ_t increase is required. For example, for $N = 50$ and a target SER equals 10^{-5}, as M changes from 4 to 64, ρ_t needs to be increased by about 13 dB.Finally, by comparing the SER of the RIS-assisted with the AF-relaying one, we observe that, in general, RIS-assisted system outperforms the AF one. Only for $N = 1$, for the same modulation scheme, in the high-SNR regime the AF-relaying wireless system achieves lower SER. However, this comparison is not fair, since the RIS-assisted system requires one timeslot to deliver the message to the final D, while the AF-relaying one needs two. Thus, the spectral efficiency of the AF-relaying system is the half of the RIS-assisted one. In other words, under the same spectral efficiency, we observe that the RIS-assisted system outpeforms the AF-relaying one in terms of SER.

Figure 7 depicts the EC as a function of ρ_t, for different values of N. In more detail, continuous lines denote the analytical results, the dashed ones illustrate the high SNR approximation, while the dashed-dotted ones the high SNR-and-N approximation. Likewise, markers are used for the Monte Carlo simulation results. For the sake of comparison, the EC of the AF-relaying wireless system is also plotted. From this figure, it becomes evident that the theoretical and simulation results match; hence, the theoretical framework is verified. Interestingly, both the high-SNR and the high-SNR-N approximations provide excellent fits even in the medium and low transmission SNR regimes. This is because of the diversity gain of the RIS-assisted wireless systems.

Likewise, we observe that, for a given N, as ρ_t increases, the EC also increases. For instance, for $N = 2$, as ρ_t increases from 5 to 10 dB, the EC improves by about 34.2%. Moreover, for a fixed ρ_t, as N increases, the EC also increases. For example, for $\rho_t = 10$ dB, as N shifts from 50 to 100, the EC increases for approximately 12.64%. Furthermore, this figure reveals that, independently of ρ_t, as N doubles, the EC increases by about 2 bits/s/Hz. Finally, it is observed that even with $N = 1$, the RIS-assisted wireless system outperforms the AF-relaying one in terms of EC.

V. CONCLUSIONS & FUTURE WORK

The present contribution investigated the efficiency of RIS-assisted wireless system in terms of average SNR, OP, SER, diversity order, and EC. In more detail, after statistically characterizing the e2e wireless channel of the RIS-assisted system, we provided novel closed-form expressions for the instantaneous and average SNR, as well as its PDF and CDF. Moreover, we extracted analytical expressions for the OP as well as the SER of a number of Gray-mapped modulation schemes. Likewise, low-complexity tight high-SNR approximations for the SER are also derived accompanied by an analytical expression for the system's diversity order. Additionally, closed-form expressions for the EC together with low-complexity tight high-SNR and high-N approximations are extracted. As a benchmark, the corresponding performance metrics of an AF-relaying wireless system was also assessed and compared. The theoretical results were compared against respective Monte Carlo simulations, which validated their accuracy. Our results revealed that as the number of MSs increases, the diversity gain and order also increase; hence, the performance of the RIS-assisted wireless systems improves. Additionally, interesting design observations were extracted. For example, it was reported that as the number of MSs, from which a RIS consists, doubles, the average e2e SNR increases for approximately 6 dB, and the EC by about 2 bits/s/Hz. Finally, it became evident that, in general, realistic RIS-assisted wireless systems clearly outperform the corresponding AF-relaying ones in terms of average SNR, OP, SER, and EC.

The performance assessment and comparison of RIS and relay-assisted wireless systems were conducted under the assumptions that (i) the intermediate channels are independent, flat, and Rayleigh distributed, and (ii) there is no direct link between S and D. It would be of high interest to relax the aforementioned assumptions and present a new comparison study. Motivated by this, our future work includes the study of RIS-assisted systems performance that operate in composite fading environments in the presence and absence of direct link between the S and D.

APPENDICES

APPENDIX A
PROOF OF THEOREM 1

From (6), $|h_i|$ and $|g_i|$ are Rayleigh distributed RVs. Hence, their product is a double Rayleigh distributed RV. As a result, A is the sum of N independent and identical double Rayleigh processes and, according to [68, ch. 2.2.2], its PDF can be tightly approximated as the first term of a Laguerre series expansion, i.e., (7), where the parameters a and b are respectively given by (9) and (10), whereas k_1 and k_2 can be obtained as [68, eq. (2.74)]

$$k_1 = \mathbb{E}[A], \tag{70}$$

and

$$k_2 = 4\mathbb{V}[A]. \tag{71}$$

The expected value of A can be analytically evaluated as

$$\mathbb{E}[A] = \mathbb{E}\left[\sum_{i=1}^{N} |h_i||g_i|\right], \tag{72}$$

or equivalently

$$\mathbb{E}[A] = \sum_{i=1}^{N} \mathbb{E}\left[|h_i||g_i|\right]. \tag{73}$$

Since $|h_i|$ and $|g_i|$ are independent RVs, (73) can be rewritten as

$$\mathbb{E}[A] = \sum_{i=1}^{N} \mathbb{E}\left[|h_i|\right]\mathbb{E}\left[|g_i|\right]. \tag{74}$$

Likewise, $|h_i|$ and $|g_i|$ follow Rayleigh distribution with variances 1; thus,

$$\mathbb{E}\left[|h_i|\right] = \mathbb{E}\left[|g_i|\right] = \sqrt{\frac{\pi}{2}}. \tag{75}$$

By substituting (75) into (74), we get

$$\mathbb{E}[A] = N\frac{\pi}{2}. \tag{76}$$

By substituting (76) into (70), we obtain (11).

Following a similar procedure, the variance of A can be obtained as

$$\mathbb{V}[A] = N\left(1 - \frac{\pi^2}{16}\right). \tag{77}$$

By substituting (77) into (71), we get (12).

Next, we express the CDF of A as

$$F_A(x) = \int_0^x f_A(y)\,\mathrm{d}y, \tag{78}$$

which, with the aid of (7), can be rewritten as

$$F_A(x) = \frac{1}{b^{a+1}\Gamma(a+1)}\mathcal{I}(x), \tag{79}$$

where

$$\mathcal{I}(x) = \int_0^x y^a \exp\left(-\frac{y}{b}\right)\mathrm{d}y, \tag{80}$$

which, by setting $z = \frac{y}{b}$ and employing [56, eq. (8.350/1)], can be written in closed-form as

$$\mathcal{I}(x) = b^{a+1}\gamma\left(a+1, \frac{x}{b}\right). \tag{81}$$

By substituting (81) into (79), we get (8). This concludes the proof.

APPENDIX B
PROOF OF THEOREM 2

With the aid of (18), the average e2e SNR can be analytically written as

$$\mathbb{E}[\rho] = \rho_s \int_0^\infty x^2 f_A(x)\, \mathrm{d}x, \tag{82}$$

which, by substituting (7), can be expressed as

$$\mathbb{E}[\rho] = \frac{\rho_s}{b^{a+1}\Gamma(a+1)} \mathcal{J}, \tag{83}$$

where

$$\mathcal{J} = \int_0^\infty x^{a+2} \exp\left(-\frac{x}{b}\right) \mathrm{d}x. \tag{84}$$

By employing [56, eq. (8.310/1)], (84) can be written in closed-form as

$$\mathcal{J} = b^{a+3}\Gamma(a+3). \tag{85}$$

By substituting (85) into (83), we obtain (20). This concludes the proof.

APPENDIX C
PROOF OF THEOREM 3

The CDF of ρ can be expressed as [69]

$$F_\rho(x) = \Pr(\rho \leq x). \tag{86}$$

By employing (18), (86) can be re-written as

$$F_\rho(x) = \Pr\left(A \leq \sqrt{\frac{x}{\rho_s}}\right), \tag{87}$$

or equivalently

$$F_\rho(x) = F_A\left(\sqrt{\frac{x}{\rho_s}}\right), \tag{88}$$

which, by using (8), returns (25). Next, we obtain the PDF of ρ through the derivation of (25), i.e,

$$f_\rho(x) = \frac{\mathrm{d}F_\rho(x)}{\mathrm{d}x}. \tag{89}$$

This concludes the proof.

APPENDIX D
PROOF OF LEMMA 1

According to (88), the CDF of ρ^s can be obtained as

$$F^s_\rho(x) = F^s_A\left(\sqrt{\frac{x}{\rho_s}}\right), \tag{90}$$

or, by employing (14), as in (26). Moreover, the PDF of ρ^s, can be obtained as

$$f^s_\rho(x) = \frac{\mathrm{d}F^s_\rho(x)}{\mathrm{d}x}, \tag{91}$$

which, by substituting (26) and performing the derivation, yields (27). This concludes the proof.

APPENDIX E
PROOF OF LEMMA 2

For the special case in which $N = 1$, the average e2e SNR can be evaluated as

$$\mathbb{E}\left[\rho^s\right] = \int_0^\infty x f^s_\rho(x)\, \mathrm{d}x, \tag{92}$$

which, by employing (13) and after some algebraic manipulations, can be rewritten as

$$\mathbb{E}\left[\rho^s\right] = \frac{1}{4\rho_s}\mathcal{N}_1 - \frac{1}{2\sqrt{\rho_s}}\mathcal{N}_2 + \frac{1}{4\rho_s}\mathcal{N}_3, \tag{93}$$

where

$$\mathcal{N}_1 = \int_0^\infty x K_0\left(\sqrt{\frac{x}{\rho_s}}\right) \mathrm{d}x, \tag{94}$$

$$\mathcal{N}_2 = \int_0^\infty \sqrt{x} K_1\left(\sqrt{\frac{x}{\rho_s}}\right) \mathrm{d}x, \tag{95}$$

and

$$\mathcal{N}_3 = \int_0^\infty x K_2\left(\sqrt{\frac{x}{\rho_s}}\right) \mathrm{d}x. \tag{96}$$

By setting $z = \sqrt{\frac{x}{\rho_s}}$ in (94)-(96) and employing [70, Eq. (5.3)], we get

$$\mathcal{N}_1 = 8\rho_s^2, \tag{97}$$

$$\mathcal{N}_2 = 4\rho_s^{3/2} \tag{98}$$

and

$$\mathcal{N}_3 = 16\rho_s^2. \tag{99}$$

Finally, by substituting (97)-(99) into (93), we get (28). This concludes the proof.

APPENDIX F
PROOF OF THEOREM 4

By assuming a two-dimensional modulation, the conditional to the received SNR, ρ, SER can be obtained as [71]

$$P_{e|\rho}(x) = c\, \mathrm{Q}\left(\sqrt{2dx}\right), \tag{100}$$

where x is the received SNR. Therefore, the average SER can be obtained as

$$P_e = \int_0^\infty P_{e|\rho}(x) f_\rho(x)\, \mathrm{d}x. \tag{101}$$

By substituting (24) and (100) into (101), the average SER can be rewritten as

$$P_e = c \frac{1}{2\, b^{a+1}\Gamma(a+1)\, \rho_s^{\frac{a+1}{2}}} \mathcal{L}, \tag{102}$$

where

$$\mathcal{L} = \int_0^\infty x^{\frac{a-1}{2}} \exp\left(-\frac{1}{b}\sqrt{\frac{x}{\rho_s}}\right) \mathrm{Q}\left(\sqrt{2\,dx}\right) \mathrm{d}x. \tag{103}$$

By employing [72, Eq. (B.112)], (103) can be equivalently expressed as

$$\mathcal{L} = \frac{1}{2}(\mathcal{L}_1 - \mathcal{L}_2), \tag{104}$$

where

$$\mathcal{L}_1 = \int_0^\infty x^{\frac{a-1}{2}} \exp\left(-\frac{1}{b}\sqrt{\frac{x}{\rho_s}}\right) \mathrm{dx} \tag{105}$$

and

$$\mathcal{L}_2 = \int_0^\infty x^{\frac{a-1}{2}} \exp\left(-\frac{1}{b}\sqrt{\frac{x}{\rho_s}}\right) \mathrm{erf}\left(\sqrt{dx}\right) \mathrm{dx}. \tag{106}$$

By setting $z = \sqrt{x}$, (105) and (106) can be respectively simplified as

$$\mathcal{L}_1 = 2\int_0^\infty z^a \exp\left(-\frac{1}{b\sqrt{\rho_s}}z\right) \mathrm{dz} \tag{107}$$

and

$$\mathcal{L}_2 = 2\int_0^\infty z^a \exp\left(-\frac{1}{b\sqrt{\rho_s}}z\right) \mathrm{erf}\left(\sqrt{d}z\right) \mathrm{dz}, \tag{108}$$

which, by respectively employing [56, Eq. (8.310/1)] and [73, eq. (06.25.21.0131.01)], can be analytically evaluated as

$$\mathcal{L}_1 = 2b^{a+1}\rho_s^{\frac{a+1}{2}}\Gamma(a+1) \tag{109}$$

and (110), as shown at the bottom of the next page. By substituting (109) and (110) into (104), we can rewrite $\mathcal{L}$ as in (111), as shown at the bottom of the next page. Finally, by substituting (111) into (102), we get (35). This concludes the proof.

APPENDIX G
PROOF OF LEMMA 3

Based on (101), the average SER can be expressed as

$$P_e^s = \int_0^\infty P_{e|\rho}(x) f_\rho^s(x) \,\mathrm{dx}, \tag{112}$$

which, by applying the integration by parts method and after some mathematical manipulations, can be equivalently written as

$$P_e^s = -\int_0^\infty F_\rho^s(x) f_e(x) \,\mathrm{dx}. \tag{113}$$

Note that, in (113), $f_e(x)$ is defined as

$$f_e(x) = \frac{\mathrm{d}P_{e|\rho}(x)}{\mathrm{dx}}, \tag{114}$$

or

$$f_e(x) = -\frac{c}{2}\sqrt{\frac{d}{4\pi}}x^{-1/2}\exp\left(-dx\right). \tag{115}$$

By substituting (26) and (115), we get

$$P_e^s = -\mathcal{P}_1 + \frac{c}{2}\sqrt{\frac{d}{4\pi\rho_s}}\mathcal{P}_2. \tag{116}$$

where

$$\mathcal{P}_1 = \int_0^\infty f_e(x) \,\mathrm{dx} \tag{117}$$

and

$$\mathcal{P}_2 = \int_0^\infty \exp\left(-dx\right) \mathrm{K}_1\left(\sqrt{x}\rho_s\right) \mathrm{dx}. \tag{118}$$

Notice that

$$\mathcal{P}_1 = 1. \tag{119}$$

Moreover, in (118), by setting $z = \rho_s\sqrt{x}$, performing integration by parts and using [58, Eq. (13.3.4)], it can be analytically obtained as

$$\mathcal{P}_2 = \frac{\pi}{2}\sqrt{\frac{\rho_s}{d}}\mathrm{U}\left(\frac{1}{2}, 0, \frac{1}{4d\rho_s}\right). \tag{120}$$

Hence,by employing (119) and (120), (116) can be finally rewritten as in (42). This concludes the proof.

APPENDIX H
PROOF OF THEOREM 5

According to (36), in the high-SNR regime the SER can be written as

$$P_{e,s} \approx \mathcal{B}_1\rho_s^{-\frac{a+1}{2}} + \mathcal{B}_2\rho_s^{-\frac{a+2}{2}} + \mathcal{B}_3\rho_s^{-\frac{a+3}{2}} + \mathcal{B}_4\rho_s^{-\frac{a+4}{2}}, \tag{121}$$

where

$$\mathcal{B}_1 = \frac{c}{2\sqrt{\pi}(a+1)b^{a+1}d^{\frac{a+1}{2}}}\frac{\Gamma\left(\frac{a+3}{4}\right)}{\Gamma(a+1)}, \tag{122}$$

$$\mathcal{B}_2 = -\frac{c}{2\sqrt{\pi}(a+2)b^{a+2}d^{\frac{a+2}{2}}}\frac{\Gamma\left(\frac{a+4}{4}\right)}{\Gamma\left(a+1\right)}, \tag{123}$$

$$\mathcal{B}_3 = \frac{c}{4\sqrt{\pi}(a+3)b^{a+3}d^{\frac{a+3}{2}}}\frac{\Gamma\left(\frac{a+5}{4}\right)}{\Gamma(a+1)} \tag{124}$$

and

$$\mathcal{B}_4 = -\frac{c}{12\sqrt{\pi}(a+4)b^{a+4}d^{\frac{a+4}{2}}}\frac{\Gamma\left(\frac{a+5}{4}\right)}{\Gamma\left(a+1\right)}. \tag{125}$$

Note that, from (122)-(125), it is evident that the terms $\mathcal{B}_1$, $\mathcal{B}_2$, $\mathcal{B}_3$, and $\mathcal{B}_4$ are independent from the SNR. Additionally, from (121), the terms $\rho_s^{-\frac{a+1}{2}}$, $\rho_s^{-\frac{a+2}{2}}$, $\rho_s^{-\frac{a+3}{2}}$, and $\rho_s^{-\frac{a+4}{2}}$ contribute with diversity order of $\frac{a+1}{2}$, $\frac{a+2}{2}$, $\frac{a+3}{2}$, and $\frac{a+4}{2}$, respectively. Thus, the diversity order can be obtained as

$$D = \min\left(\frac{a+1}{2}, \frac{a+2}{2}, \frac{a+3}{2}, \frac{a+4}{2}\right). \tag{126}$$

Note that, according to (9), (11) and (12), a can be expressed as

$$a = N\frac{\pi^2}{16-\pi^2} - 1, \tag{127}$$

which, since $N \geq 1$, is always positive. Thus, (126) can be simplified as

$$D = \frac{a+1}{2}, \tag{128}$$

which, by employing (127), can be finally written as in (43). This concludes the proof.

APPENDIX I
PROOF OF THEOREM 6

The EC is defined as

$$C = \mathbb{E}\left[\log_2\left(1+\rho\right)\right], \tag{129}$$

or, by employing (18), can be rewritten as

$$C = \mathbb{E}\left[\log_2\left(1+\rho_s A^2\right)\right], \tag{130}$$

or equivalently

$$C = \int_0^\infty \log_2\left(1+\rho_s y^2\right) f_A(y)\,\mathrm{d}y. \tag{131}$$

By substituting (7) into (131), the EC can be rewritten as

$$C = \frac{x^a}{b^{a+1}\Gamma(a+1)}\int_0^\infty \exp\left(-\frac{y}{b}\right)\log_2\left(1+\rho_s y^2\right)\,\mathrm{d}y, \tag{132}$$

or equivalently

$$C = \frac{1}{b^{a+1}\ln(2)\,\Gamma(a+1)}\mathcal{K}, \tag{133}$$

where

$$\mathcal{K} = \int_0^\infty y^a \exp\left(-\frac{y}{b}\right)\ln\left(1+\rho_s y^2\right)\,\mathrm{d}y. \tag{134}$$

According to [58, eq. (15.1.1)],

$$\ln(x) = (x-1)\,{}_2F_1\left(1,1;2;1-x\right). \tag{135}$$

By setting $x = \rho_s y^2$ in (135) and substituting the resulting expression in (134), we obtain

$$\mathcal{K} = \rho_s\int_0^\infty y^{a+2}\exp\left(-\frac{y}{b}\right)\,{}_2F_1\left(1,1;2;-\rho_s y^2\right)\,\mathrm{d}y. \tag{136}$$

Additionally, by applying integration by parts as well as [74, eq. (07.23.21.0015.01)], (134) can be expressed in closed-form as in (137), as shown at the bottom of the next page. Likewise, by substituting (137) into (133), and after some algebraic manipulations, we extract (138), as shown at the bottom of the next page. Finally, by taking into account that $\frac{\Gamma(x+n)}{\Gamma(x)} = (x)_n$, (138) can be rewritten as in (44). This concludes the proof.

APPENDIX J
PROOF OF THEOREM 7

According to [56, eq. (8.352/2)], (136) can be equivalently expressed as

$$\mathcal{K} = \rho_s\int_0^\infty y^{a+2}\Gamma\left(1,\frac{y}{b}\right)\,{}_2F_1\left(1,1;2;-\rho_s y^2\right)\,\mathrm{d}y, \tag{139}$$

which, based on [75, eq. (5)] and [76, eq. (17)], can be rewritten as

$$\mathcal{K} = 2\rho_s\times\int_0^\infty y^{a+2}G_{1,2}^{2,0}\left[\frac{y}{b}\middle|\begin{matrix}1\\0,1\end{matrix}\right]G_{2,2}^{1,2} \times\left[\rho_s y^2\middle|\begin{matrix}0,0\\0,-1\end{matrix}\right]\mathrm{d}y, \tag{140}$$

$$\begin{aligned}\mathcal{L}_2 = {} & 2b^{a+1}\rho_s^{\frac{a+1}{2}}\Gamma(a+1) - \frac{2\Gamma\left(\frac{a+3}{4}\right)}{\sqrt{\pi}(a+1)d^{\frac{a+1}{2}}}\,{}_2F_4\left(\frac{a+1}{4},\frac{a+3}{4};\frac{1}{4},\frac{1}{2},\frac{3}{4},\frac{a+5}{4};\frac{1}{256b^4d^2\rho_s^2}\right)\\ & + \frac{2\Gamma\left(\frac{a+4}{4}\right)}{\sqrt{\pi}(a+1)bd^{\frac{a+2}{2}}r^{1/2}}\,{}_2F_4\left(\frac{a+2}{4},\frac{a+4}{4};\frac{1}{2},\frac{3}{4},\frac{5}{4},\frac{a+6}{4};\frac{1}{256b^4d^2\rho_s^2}\right)\\ & - \frac{\Gamma\left(\frac{a+5}{4}\right)}{\sqrt{\pi}(a+3)b^2d^{\frac{a+3}{2}}r}\,{}_2F_4\left(\frac{a+3}{4},\frac{a+5}{4};\frac{3}{4},\frac{5}{4},\frac{3}{2},\frac{a+7}{4};\frac{1}{256b^4d^2\rho_s^2}\right)\\ & + \frac{\Gamma\left(\frac{a+6}{4}\right)}{3\sqrt{\pi}(a+4)b^3d^{\frac{a+4}{2}}\rho_s^{3/2}}\,{}_2F_4\left(\frac{a+4}{4},\frac{a+6}{4};\frac{5}{4},\frac{3}{2},\frac{7}{4},\frac{a+8}{4};\frac{1}{256b^4d^2\rho_s^2}\right)\end{aligned} \tag{110}$$

$$\begin{aligned}\mathcal{L} = {} & \frac{\Gamma\left(\frac{a+3}{4}\right)}{\sqrt{\pi}(a+1)d^{\frac{a+1}{2}}}\,{}_2F_4\left(\frac{a+1}{4},\frac{a+3}{4};\frac{1}{4},\frac{1}{2},\frac{3}{4},\frac{a+5}{4};\frac{1}{256b^4d^2\rho_s^2}\right)\\ & - \frac{\Gamma\left(\frac{a+4}{4}\right)}{\sqrt{\pi}(a+1)bd^{\frac{a+2}{2}}r^{1/2}}\,{}_2F_4\left(\frac{a+2}{4},\frac{a+4}{4};\frac{1}{2},\frac{3}{4},\frac{5}{4},\frac{a+6}{4};\frac{1}{256b^4d^2\rho_s^2}\right)\\ & + \frac{\Gamma\left(\frac{a+5}{4}\right)}{2\sqrt{\pi}(a+3)b^2d^{\frac{a+3}{2}}r}\,{}_2F_4\left(\frac{a+3}{4},\frac{a+5}{4};\frac{3}{4},\frac{5}{4},\frac{3}{2},\frac{a+7}{4};\frac{1}{256b^4d^2\rho_s^2}\right)\\ & - \frac{\Gamma\left(\frac{a+6}{4}\right)}{6\sqrt{\pi}(a+4)b^3d^{\frac{a+4}{2}}\rho_s^{3/2}}\,{}_2F_4\left(\frac{a+4}{4},\frac{a+6}{4};\frac{5}{4},\frac{3}{2},\frac{7}{4},\frac{a+8}{4};\frac{1}{256b^4d^2\rho_s^2}\right)\end{aligned} \tag{111}$$

which, with the aid of [77, ch. 2.3], can be expressed in closed-form as in (141), as shown at the bottom of this page. By substituting (141) into (133), we obtain (45). This concludes the proof.

APPENDIX K
PROOF OF LEMMA 4

According to (130), the EC can be expressed as

$$C_s = \int_0^\infty \log_2\left(1+\rho_s x\right) f_\rho^s(x)\,\mathrm{d}x, \tag{142}$$

or equivalently

$$C_s = \frac{1}{\ln(2)}\int_0^\infty \ln\left(1+\rho_s x\right) f_\rho^s(x)\,\mathrm{d}x, \tag{143}$$

which, with the aid of (27), can be rewritten as

$$C_s = \frac{1}{4\ln(2)\rho_s}\mathcal{C}_1 - \frac{1}{2\ln(2)\sqrt{\rho_s}}\mathcal{C}_2 + \frac{1}{4\ln(2)\rho_s}\mathcal{C}_3, \tag{144}$$

where

$$\mathcal{C}_1 = \int_0^\infty K_0\left(\sqrt{\frac{x}{\rho_s}}\right)\ln\left(1+\rho_s x\right)\,\mathrm{d}x, \tag{145}$$

$$\mathcal{C}_2 = \int_0^\infty x^{-1/2}K_1\left(\sqrt{\frac{x}{\rho_s}}\right)\ln\left(1+\rho_s x\right)\,\mathrm{d}x \tag{146}$$

and

$$\mathcal{C}_3 = \int_0^\infty K_2\left(\sqrt{\frac{x}{\rho_s}}\right)\ln\left(1+\rho_s x\right)\,\mathrm{d}x. \tag{147}$$

Moreover, by using [56, eq. (8.352/2)], (145)-(147) can be equivalently written as

$$\mathcal{C}_1 = \rho_s\int_0^\infty xK_0\left(\sqrt{\frac{x}{\rho_s}}\right){}_2F_1\left(1,1;2;\rho_s x\right)\,\mathrm{d}x, \tag{148}$$

$$\mathcal{C}_2 = \rho_s\int_0^\infty x^{1/2}K_1\left(\sqrt{\frac{x}{\rho_s}}\right){}_2F_1\left(1,1;2;\rho_s x\right)\,\mathrm{d}x \tag{149}$$

and

$$\mathcal{C}_3 = \rho_s\int_0^\infty xK_2\left(\sqrt{\frac{x}{\rho_s}}\right){}_2F_1\left(1,1;2;\rho_s x\right)\,\mathrm{d}x. \tag{150}$$

Additionally, with the aid of [78, eq. (03.04.26.0009.01)] and [76, eq. (17)], (148)-(150) can be respectively expressed as

$$\mathcal{C}_1 = \frac{\rho_s}{2}\int_0^\infty xG_{0,2}^{2,0}\left(\frac{x}{4\rho_s}\middle|0,0\right) \times G_{2,2}^{1,2}\left(\rho_s x\middle|\begin{matrix}0,0\\0,-1\end{matrix}\right)\mathrm{d}x, \tag{151}$$

$$\mathcal{C}_2 = \frac{\rho_s}{2}\int_0^\infty x^{1/2}G_{0,2}^{2,0}\left(\frac{x}{4\rho_s}\middle|\frac{1}{2},-\frac{1}{2}\right) \times G_{2,2}^{1,2}\left(\rho_s x\middle|\begin{matrix}0,0\\0,-1\end{matrix}\right)\mathrm{d}x \tag{152}$$

and

$$\mathcal{C}_3 = \frac{\rho_s}{2}\int_0^\infty xG_{0,2}^{2,0}\left(\frac{x}{4\rho_s}\middle|1,-1\right) \times G_{2,2}^{1,2}\left(\rho_s x\middle|\begin{matrix}0,0\\0,-1\end{matrix}\right)\mathrm{d}x. \tag{153}$$

By employing [77, ch. 2.3], (151)-(153) can be analytically obtained as

$$\mathcal{C}_1 = \frac{1}{2\rho_s}G_{1,3}^{3,1}\left(\frac{1}{4\rho_s^2}\middle|\begin{matrix}-1\\-1,-1,0\end{matrix}\right), \tag{154}$$

$$\mathcal{C}_2 = \frac{1}{2\sqrt{\rho_s}}G_{1,3}^{3,1}\left(\frac{1}{4\rho_s^2}\middle|\begin{matrix}-\frac{1}{2}\\-\frac{1}{2},-\frac{1}{2},-\frac{1}{2}\end{matrix}\right) \tag{155}$$

$$\begin{aligned}\mathcal{K} = {} & 4\,ab^{a+3}\Gamma(a)\rho_s\ln\left(b\sqrt{\rho_s}\right) + 6\,a^2\,b^{a+3}\Gamma(a)\rho_s\ln\left(b\sqrt{\rho_s}\right) + 2\,a^3\,b^{a+3}\Gamma(a)\rho_s\ln\left(b\sqrt{\rho_s}\right)\\ & + 2\,a(a+1)(a+2)b^{a+3}\Gamma(a)F_0\left(3+a\right) - \frac{\pi}{(4+a)b\rho_s^{\frac{a}{2}+1}}\csc\left(\frac{a\pi}{2}\right){}_1F_2\left(2+\frac{a}{2};\frac{3}{2},3+\frac{a}{2},-\frac{1}{4\,b^2\rho_s}\right)\\ & - \frac{\pi}{(a+3)\rho_s^{\frac{a+1}{2}}}\sec\left(\frac{a\pi}{2}\right){}_1F_2\left(\frac{a+3}{2};\frac{1}{2},\frac{a+5}{2},-\frac{1}{4b^2\rho_s}\right) + ab^{a+1}\Gamma(a)\,{}_2F_3\left(1,1;2,\frac{1-a}{2},-\frac{a}{2},-\frac{1}{4b^2\rho_s}\right)\end{aligned} \tag{137}$$

$$\begin{aligned}C = {} & 4\,ab^2\frac{\Gamma(a)}{\Gamma(a+1)}\rho_s\log_2\left(b\sqrt{\rho_s}\right) + 6\,a^2\,b^2\frac{\Gamma(a)}{\Gamma(a+1)}\rho_s\log_2\left(b\sqrt{\rho_s}\right) + 2\,a^3\,b^2\frac{\Gamma(a)}{\Gamma(a+1)}\rho_s\log_2\left(b\sqrt{\rho_s}\right)\\ & + \frac{2}{\ln(2)}a(a+1)(a+2)b^2\frac{\Gamma(a)}{\Gamma(a+1)}F_0\left(3+a\right) - \frac{\pi}{\ln(2)(4+a)b^{a+2}\Gamma(a+1)\rho_s^{\frac{a}{2}+1}}\csc\left(\frac{a\pi}{2}\right){}_1F_2\left(2+\frac{a}{2};\frac{3}{2},3+\frac{a}{2},-\frac{1}{4\,b^2\rho_s}\right)\\ & - \frac{\pi}{(a+3)b^{a+1}\ln(2)\,\Gamma(a+1)\rho_s^{\frac{a+1}{2}}}\sec\left(\frac{a\pi}{2}\right){}_1F_2\left(\frac{a+3}{2};\frac{1}{2},\frac{a+5}{2},-\frac{1}{4b^2\rho_s}\right)\\ & + \frac{a}{\ln(2)}\frac{\Gamma(a)}{\Gamma(a+1)}\,{}_2F_3\left(1,1;2,\frac{1-a}{2},-\frac{a}{2},-\frac{1}{4b^2\rho_s}\right)\end{aligned} \tag{138}$$

$$\mathcal{K} = 2b^{a+3}\rho_s H_{4,3}^{1,4}\left[b^2\rho_s\middle|\begin{matrix}(0,1),(0,1),(-a-2,2),(-a-3,2)\\(0,1),(-a-3,2),(-1,1)\end{matrix}\right] \tag{141}$$

and

$$\mathcal{C}_3 = \frac{1}{2\rho_s} G_{2,4}^{4,1}\left(\frac{1}{4\rho_s^2}\middle| \begin{matrix} -1, 0 \\ -1, -1, -1, 1 \end{matrix}\right). \quad (156)$$

Finally, by substituting (154)-(156) into (144), we extract (53). This concludes the proof.

APPENDIX L
PROOF OF LEMMA 5

In the case of AF-relaying wireless system, the average e2e SNR can be obtained as

$$\mathbb{E}[\rho_r] = \int_0^\infty x f_{\rho_r}(x)\, \mathrm{dx}, \quad (157)$$

which, by substituting (59), can be rewritten as

$$\mathbb{E}[\rho_r] = \beta\gamma\mathcal{M}_1 + \gamma^2\mathcal{M}_2, \quad (158)$$

where

$$\mathcal{M}_1 = \int_0^\infty x^2 \exp\left(-\beta x\right) K_1\left(\gamma x\right)\, \mathrm{dx} \quad (159)$$

and

$$\mathcal{M}_2 = \int_0^\infty x^2 \exp\left(-\beta x\right) K_0\left(\gamma x\right)\, \mathrm{dx}. \quad (160)$$

Next, we deliver closed-form expressions for (159) and (160). In particular, for $\beta \neq \gamma$, by employing [56, eq. (6.621/3)] and [56, eq. (6.624/1)], (159) and (160) can be respectively expressed as

$$M_1 = -\frac{\beta^4}{\gamma\left(-\beta^2+\gamma^2\right)^3} + \frac{2\gamma^3-\beta^2\gamma}{\left(-\beta^2+\gamma^2\right)^3} - \frac{3\pi\beta\gamma}{2\left(-\beta^2+\gamma^2\right)^{5/2}} + \frac{3\beta\gamma}{\left(-\beta^2+\gamma^2\right)^{5/2}}\mathrm{acsc}\left(\frac{\gamma}{\beta}\right) \quad (161)$$

and

$$\mathcal{M}_2 = -\frac{3\beta}{\left(-\beta^2+\gamma^2\right)^2} + \frac{\pi}{2}\frac{2\beta^2+\gamma^2}{\left(-\beta^2+\gamma^2\right)^{5/2}} - \frac{2\beta}{\left(-\beta^2+\gamma^2\right)^{5/2}}\mathrm{acsc}\left(\frac{\gamma}{\beta}\right). \quad (162)$$

Finally, by substituting (161) and (162) into (158), we get (63).

On the contrary, for $\beta = \gamma$, (159) and (160) can be respectively written as

$$\mathcal{M}_1 = \int_0^\infty x^2 \exp\left(-\beta x\right) K_1\left(\beta x\right)\, \mathrm{dx} \quad (163)$$

and

$$\mathcal{M}_2 = \int_0^\infty x^2 \exp\left(-\beta x\right) K_0\left(\beta x\right)\, \mathrm{dx}. \quad (164)$$

which by employing [56, eq. (6.621/3)] and after some algebraic manipulations, can be obtained as

$$\mathcal{M}_1 = \frac{2}{5\gamma^3} \quad (165)$$

and

$$\mathcal{M}_2 = \frac{4}{15\gamma^3}. \quad (166)$$

Finally, by substituting (165) and (166) into (158), we obtain (64). This concludes the proof.

APPENDIX M
PROOF OF LEMMA 6

In the case of AF-relaying wireless system, based on (113), the SER can be analytically evaluated as

$$P_e^{\mathrm{AF}} = -\int_0^\infty F_{\rho_r}(x) f_e(x)\, \mathrm{dx}, \quad (167)$$

which, by using (60) and (115), can be rewritten as

$$P_e^{\mathrm{AF}} = -1 - \frac{\gamma c}{2}\sqrt{\frac{d}{4\pi}}\mathcal{D}, \quad (168)$$

where

$$\mathcal{D} = \int_0^\infty x^{1/2} \exp\left(-\left(\beta+d\right)x\right) K_1\left(\gamma x\right)\, \mathrm{dx}. \quad (169)$$

By employing [79, p. 185], (169) can be expressed as

$$\mathcal{D} = \frac{\pi}{2}\left(\mathcal{D}_1 - \mathcal{D}_2\right), \quad (170)$$

where

$$\mathcal{D}_1 = \int_0^\infty x^{1/2} \exp\left(-\left(\beta+d\right)x\right) I_1\left(\gamma x\right)\, \mathrm{dx} \quad (171)$$

and

$$\mathcal{D}_2 = \int_0^\infty x^{1/2} \exp\left(-\left(\beta+d\right)x\right) I_{-1}\left(\gamma x\right)\, \mathrm{dx}. \quad (172)$$

Next, by applying [56, eq. (6.622)] into (171) and (172), we obtain

$$\mathcal{D}_1 = \sqrt{\frac{2}{\pi}}\frac{\beta+\gamma+d}{\sqrt{\gamma}\left(\gamma^2-(\beta+d)^2\right)}\mathrm{K}\left(\frac{1}{2}-\frac{\beta+d}{2\gamma}\right) \quad (173)$$

and

$$\mathcal{D}_2 = -2\sqrt{\frac{2}{\pi}}\frac{\beta+d}{\sqrt{\gamma}\left(\gamma^2-(\beta+d)^2\right)} \times \mathrm{E}\left(\frac{1}{2}-\frac{\beta+d}{2\gamma}\right). \quad (174)$$

Next, by substituting (173) and (174) into (170), we derive

$$\mathcal{D} = -2\sqrt{\frac{\pi}{2}}\frac{\beta+d}{\sqrt{\gamma}\left(\gamma^2-(\beta+d)^2\right)}\mathrm{E}\left(\frac{1}{2}-\frac{\beta+d}{2\gamma}\right) + \sqrt{\frac{\pi}{2}}\frac{\beta+\gamma+d}{\sqrt{\gamma}\left(\gamma^2-(\beta+d)^2\right)}\mathrm{K}\left(\frac{1}{2}-\frac{\beta+d}{2\gamma}\right). \quad (175)$$

Finally, by substituting (175) into (168), we obtain (68). This concludes the proof.

APPENDIX N
PROOF OF LEMMA 7

According to (130), the EC can be expressed as

$$C^{\mathrm{AF}} = \frac{1}{\ln(2)} \int_0^{\infty} \ln\left(1+x\right) f_{\rho_r}(x)\, \mathrm{d}x. \tag{176}$$

By substituting (59) in (176), we obtain

$$C^{\mathrm{AF}} = \frac{\gamma^2}{\ln(2)} \mathcal{F}_1 + \frac{\beta\gamma}{\ln(2)} \mathcal{F}_2. \tag{177}$$

where

$$\mathcal{F}_1 = \int_0^{\infty} x \exp\left(-\beta x\right) \ln(1+x) K_0\left(\gamma x\right)\ \mathrm{dx} \tag{178}$$

and

$$\mathcal{F}_2 = \int_0^{\infty} x \exp\left(-\beta x\right) \ln(1+x) K_1\left(\gamma x\right)\ \mathrm{dx}. \tag{179}$$

For $\beta \neq \gamma$, note that (178) and (179) can be equivalently written as

$$\mathcal{F}_1 = \int_0^{\infty} x \exp\left(-\left(\beta-\gamma\right)x\right) \ln(1+x) \times \exp\left(-\gamma x\right) K_0\left(\gamma x\right)\ \mathrm{dx} \tag{180}$$

and

$$\mathcal{F}_2 = \int_0^{\infty} x \exp\left(-\left(\beta-\gamma\right)x\right) \ln(1+x) \times \exp\left(-\gamma x\right) K_1\left(\gamma x\right)\ \mathrm{dx} \tag{181}$$

By employing [56, eq. (8.352/2)] and [58, eq. (15.1.1)], (180) and (181) can be respectively written as

$$\mathcal{F}_1 = \int_0^{\infty} x^2 \Gamma\left(1, (\beta-\gamma)x\right)\ {}_2F_1\left(1, 1; 2; -x\right) \times \exp\left(-\gamma x\right) K_0\left(\gamma x\right)\ \mathrm{dx} \tag{182}$$

and

$$\mathcal{F}_2 = \int_0^{\infty} x^2 \Gamma\left(1, (\beta-\gamma)x\right)\ {}_2F_1\left(1, 1; 2; -x\right) \times \exp\left(-\gamma x\right) K_1\left(\gamma x\right)\ \mathrm{dx}, \tag{183}$$

which, by using [75, eq. (20)], [76, eq. (17)] and [80] can be equivalently rewritten as

$$\mathcal{F}_1 = \sqrt{\pi} \int_0^{\infty} x^2\, G_{1,2}^{2,0}\left[\left(\beta-\gamma\right)x \,\middle|\, \begin{matrix}1\\0,1\end{matrix}\right] G_{2,2}^{1,2}\left[x \,\middle|\, \begin{matrix}0,0\\0,-1\end{matrix}\right] \times G_{1,2}^{2,0}\left[2\gamma x \,\middle|\, \begin{matrix}\frac{1}{2}\\0,0\end{matrix}\right] \mathrm{dx} \tag{184}$$

and

$$\mathcal{F}_2 = \sqrt{\pi} \int_0^{\infty} x^2\, G_{1,2}^{2,0}\left[\left(\beta-\gamma\right)x \,\middle|\, \begin{matrix}1\\0,1\end{matrix}\right] G_{2,2}^{1,2}\left[x \,\middle|\, \begin{matrix}0,0\\0,-1\end{matrix}\right] \times G_{1,2}^{2,0}\left[2\gamma x \,\middle|\, \begin{matrix}\frac{1}{2}\\-1,1\end{matrix}\right] \mathrm{dx}. \tag{185}$$

With the aid of [81], (184) and (185) can be analytically evaluated as (186) and (187), as shown at the bottom of this page. By substituting (186) and (187) into (177), we obtain (188), as shown at the bottom of this page.

Next, we examine the case in which $\beta = \gamma$. For $\beta = \gamma$, (178) and (179) can be respectively expressed as

$$\mathcal{F}_1 = \int_0^{\infty} x \ln(1+x) \exp\left(-\gamma x\right) K_0\left(\gamma x\right)\ \mathrm{dx} \tag{189}$$

and

$$\mathcal{F}_2 = \int_0^{\infty} x \ln(1+x) \exp\left(-\gamma x\right) K_1\left(\gamma x\right)\ \mathrm{dx}, \tag{190}$$

which, by following the same steps as in the case of $\beta \neq \gamma$, can be rewritten as

$$\mathcal{F}_1 = \sqrt{\pi} \int_0^{\infty} x^2 G_{2,2}^{1,2}\left[x \,\middle|\, \begin{matrix}0,0\\0,-1\end{matrix}\right] G_{1,2}^{2,0}\left[2\gamma x \,\middle|\, \begin{matrix}\frac{1}{2}\\0,0\end{matrix}\right] \mathrm{dx} \tag{191}$$

and

$$\mathcal{F}_2 = \sqrt{\pi} \int_0^{\infty} x^2 G_{2,2}^{1,2}\left[x \,\middle|\, \begin{matrix}0,0\\0,-1\end{matrix}\right] G_{1,2}^{2,0}\left[2\gamma x \,\middle|\, \begin{matrix}\frac{1}{2}\\-1,1\end{matrix}\right] \mathrm{dx}. \tag{192}$$

By employing [77, ch. 2.3], (191) and (192) can be respectively expressed as

$$\mathcal{F}_1 = \sqrt{\pi} G_{3,4}^{4,1}\left(2\gamma \,\middle|\, \begin{matrix}-2,-1,\frac{1}{2}\\0,0,-2,-2\end{matrix}\right) \tag{193}$$

and

$$\mathcal{F}_2 = \sqrt{\pi} G_{3,4}^{4,1}\left(2\gamma \,\middle|\, \begin{matrix}-2,-1,\frac{1}{2}\\-1,1,-2,-2\end{matrix}\right). \tag{194}$$

By substituting (193) and (194) into (177), we get (195), as shown at the top of the next page. Finally, by combining (188) and (195), we obtain (69). This concludes the proof.

$$\mathcal{F}_1 = \sqrt{\pi}\left(\beta-\gamma\right)^{-3} G_{2,1:2,2:1,2}^{0,2:1,2:2,0}\left(\begin{matrix}-2,-3\\-3\end{matrix}\,\middle|\,\begin{matrix}0,0\\0,-1\end{matrix}\,\middle|\,\begin{matrix}\frac{1}{2}\\0,0\end{matrix}\,\middle|\,\frac{1}{\beta-\gamma}, \frac{2\gamma}{\beta-\gamma}\right) \tag{186}$$

$$\mathcal{F}_2 = \sqrt{\pi}\left(\beta-\gamma\right)^{-3} G_{2,1:2,2:1,2}^{0,2:1,2:2,0}\left(\begin{matrix}-2,-3\\-3\end{matrix}\,\middle|\,\begin{matrix}0,0\\0,-1\end{matrix}\,\middle|\,\begin{matrix}\frac{1}{2}\\-1,-1\end{matrix}\,\middle|\,\frac{1}{\beta-\gamma}, \frac{2\gamma}{\beta-\gamma}\right) \tag{187}$$

$$C^{\mathrm{AF}} = \frac{\sqrt{\pi}}{\ln(2)} \frac{\gamma^2}{\left(\beta-\gamma\right)^3} G_{2,1:2,2:1,2}^{0,2:1,2:2,0}\left(\begin{matrix}-2,-3\\-3\end{matrix}\,\middle|\,\begin{matrix}0,0\\0,-1\end{matrix}\,\middle|\,\begin{matrix}\frac{1}{2}\\0,0\end{matrix}\,\middle|\,\frac{1}{\beta-\gamma}, \frac{2\gamma}{\beta-\gamma}\right) + \frac{\sqrt{\pi}}{\ln(2)} \frac{\beta\gamma}{\left(\beta-\gamma\right)^3} G_{2,1:2,2:1,2}^{0,2:1,2:2,0}\left(\begin{matrix}-2,-3\\-3\end{matrix}\,\middle|\,\begin{matrix}0,0\\0,-1\end{matrix}\,\middle|\,\begin{matrix}\frac{1}{2}\\-1,-1\end{matrix}\,\middle|\,\frac{1}{\beta-\gamma}, \frac{2\gamma}{\beta-\gamma}\right), \quad \text{for } \beta \neq \gamma \tag{188}$$

$$C^{\mathrm{AF}} = \frac{\sqrt{\pi}}{\ln(2)}\gamma^2 \left(G_{3,4}^{4,1}\left(2\gamma \left| \begin{matrix} -2, -1, \frac{1}{2} \\ 0, 0, -2, -2 \end{matrix} \right.\right) + G_{3,4}^{4,1}\left(2\gamma \left| \begin{matrix} -2, -1, \frac{1}{2} \\ -1, 1, -2, -2 \end{matrix} \right.\right) \right), \quad \text{for } \beta = \gamma \tag{195}$$

ACKNOWLEDGMENT

The authors would like to thank the editor and anonymous reviewers for their constructive comments and criticism.

REFERENCES

[1] W. Saad, M. Bennis, and M. Chen, "A vision of 6G wireless systems: Applications, trends, technologies, and open research problems," *IEEE Netw.*, Apr. 2020.

[2] K. David and H. Berndt, "6G vision and requirements: Is there any need for beyond 5G?" *IEEE Veh. Technol. Mag.*, vol. 13, no. 3, pp. 72–80, Sep. 2018.

[3] Z. Zhang, Y. Xiao, Z. Ma, M. Xiao, Z. Ding, X. Lei, G. K. Karagiannidis, and P. Fan, "6G wireless networks: Vision, requirements, architecture, and key technologies," *IEEE Veh. Technol. Mag.*, vol. 14, no. 3, pp. 28–41, Sep. 2019.

[4] H. Viswanathan and P. E. Mogensen, "Communications in the 6G era," *IEEE Access*, vol. 8, pp. 57063–57074, 2020.

[5] C. Pan, H. Ren, K. Wang, W. Xu, M. Elkashlan, A. Nallanathan, and L. Hanzo, "Multicell MIMO communications relying on intelligent reflecting surface," 2019, *arXiv:1907.10864*. [Online]. Available: http://arxiv.org/abs/1907.10864

[6] X. Yang, M. Matthaiou, J. Yang, C.-K. Wen, F. Gao, and S. Jin, "Hardware-constrained millimeter-wave systems for 5G: Challenges, opportunities, and solutions," *IEEE Commun. Mag.*, vol. 57, no. 1, pp. 44–50, Jan. 2019.

[7] A.-A.-A. Boulogeorgos and G. K. Karagiannidis, "Energy detection in full-duplex systems with residual RF impairments over fading channels," *IEEE Wireless Commun. Lett.*, vol. 7, no. 2, pp. 246–249, Apr. 2018.

[8] A.-A. A. Boulogeorgos, "Interference mitigation techniques in modern wireless communication systems," Ph.D. dissertation, Dept. Elect. Comput. Eng., Aristotle Univ. Thessaloniki, Thessaloniki, Greece, Sep. 2016.

[9] Y. Han, W. Tang, S. Jin, C.-K. Wen, and X. Ma, "Large intelligent surface-assisted wireless communication exploiting statistical CSI," *IEEE Trans. Veh. Technol.*, vol. 68, no. 8, pp. 8238–8242, Aug. 2019.

[10] S. Hu, F. Rusek, and O. Edfors, "Beyond massive MIMO: The potential of data transmission with large intelligent surfaces," *IEEE Trans. Signal Process.*, vol. 66, no. 10, pp. 2746–2758, May 2018.

[11] M. D. Renzo, M. Debbah, D.-T. Phan-Huy, A. Zappone, M.-S. Alouini, C. Yuen, V. Sciancalepore, G. C. Alexandropoulos, J. Hoydis, H. Gacanin, J. D. Rosny, A. Bounceur, G. Lerosey, and M. Fink, "Smart radio environments empowered by reconfigurable AI meta-surfaces: An idea whose time has come," *EURASIP J. Wireless Commun. Netw.*, vol. 2019, no. 1, pp. 1–20, Dec. 2019.

[12] C. Liaskos, A. Tsioliaridou, A. Pitsillides, S. Ioannidis, and I. Akyildiz, "Using any surface to realize a new paradigm for wireless communications," *Commun. ACM*, vol. 61, no. 11, pp. 30–33, Oct. 2018, doi: 10.1145/3192336.

[13] A. C. Tasolamprou *et al.*, "Exploration of intercell wireless millimeter-wave communication in the landscape of intelligent metasurfaces," *IEEE Access*, vol. 7, pp. 122931–122948, Aug. 2019.

[14] Q. Wu and R. Zhang, "Intelligent reflecting surface enhanced wireless network: Joint active and passive beamforming design," in *Proc. IEEE Global Commun. Conf. (GLOBECOM)*, Dec. 2018, pp. 1–6.

[15] E. Basar, M. Di Renzo, J. De Rosny, M. Debbah, M.-S. Alouini, and R. Zhang, "Wireless communications through reconfigurable intelligent surfaces," *IEEE Access*, vol. 7, pp. 116753–116773, 2019.

[16] C. Huang, A. Zappone, G. C. Alexandropoulos, M. Debbah, and C. Yuen, "Reconfigurable intelligent surfaces for energy efficiency in wireless communication," *IEEE Trans. Wireless Commun.*, vol. 18, no. 8, pp. 4157–4170, Aug. 2019.

[17] H. Lang and C. D. Sarris, "Optimization of wireless power transfer systems enhanced by passive elements and metasurfaces," *IEEE Trans. Antennas Propag.*, vol. 65, no. 10, pp. 5462–5474, Oct. 2017.

[18] N. Kaina, M. Dupré, G. Lerosey, and M. Fink, "Shaping complex microwave fields in reverberating media with binary tunable metasurfaces," *Sci. Rep.*, vol. 4, no. 1, p. 6693, May 2015.

[19] H. Yang, X. Cao, F. Yang, J. Gao, S. Xu, M. Li, X. Chen, Y. Zhao, Y. Zheng, and S. Li, "A programmable metasurface with dynamic polarization, scattering and focusing control," *Sci. Rep.*, vol. 6, no. 1, p. 35692, Dec. 2016.

[20] L. Subrt and P. Pechac, "Controlling propagation environments using intelligent walls," in *Proc. 6th Eur. Conf. Antennas Propag. (EUCAP)*, Mar. 2012, pp. 1–5.

[21] M. Akbari, F. Samadi, A.-R. Sebak, and T. A. Denidni, "Superbroadband diffuse wave scattering based on coding metasurfaces: Polarization conversion metasurfaces," *IEEE Antennas Propag. Mag.*, vol. 61, no. 2, pp. 40–52, Apr. 2019.

[22] X. Ding, H. Yu, S. Zhang, Y. Wu, K. Zhang, and Q. Wu, "Ultrathin metasurface for controlling electromagnetic wave with broad bandwidth," *IEEE Trans. Magn.*, vol. 51, no. 11, pp. 1–4, Nov. 2015.

[23] S. V. Hum and J. Perruisseau-Carrier, "Reconfigurable reflectarrays and array lenses for dynamic antenna beam control: A review," *IEEE Trans. Antennas Propag.*, vol. 62, no. 1, pp. 183–198, Jan. 2014.

[24] X. Tan, Z. Sun, J. M. Jornet, and D. Pados, "Increasing indoor spectrum sharing capacity using smart reflect-array," in *Proc. IEEE Int. Conf. Commun. (ICC)*, May 2016, pp. 1–6.

[25] X. Tan, Z. Sun, D. Koutsonikolas, and J. M. Jornet, "Enabling indoor mobile millimeter-wave networks based on smart reflect-arrays," in *Proc. IEEE Conf. Comput. Commun. (INFOCOM)*, Apr. 2018, pp. 270–278.

[26] L. Li, H. Ruan, C. Liu, Y. Li, Y. Shuang, A. Alù, C.-W. Qiu, and T. J. Cui, "Machine-learning reprogrammable metasurface imager," *Nature Commun.*, vol. 10, no. 1, pp. 1–8, Dec. 2019.

[27] M. Jung, W. Saad, Y. Jang, G. Kong, and S. Choi, "Performance analysis of large intelligent surfaces (LISs): Asymptotic data rate and channel hardening effects," *CoRR*, vol. abs/1810.05667, Oct. 2018. [Online]. Available: http://arxiv.org/abs/1810.05667

[28] Q. Wu and R. Zhang, "Beamforming optimization for intelligent reflecting surface with discrete phase shifts," in *Proc. IEEE Int. Conf. Acoust., Speech Signal Process. (ICASSP)*, May 2019, pp. 7830–7833.

[29] Q. Nadeem, A. Kammoun, A. Chaaban, M. Debbah, and M. Alouini, "Asymptotic analysis of large intelligent surface assisted MIMO communication," *CoRR*, vol. abs/1903.08127, Apr. 2019. [Online]. Available: http://arxiv.org/abs/1903.08127

[30] C. Pan, H. Ren, K. Wang, M. Elkashlan, A. Nallanathan, J. Wang, and L. Hanzo, "Intelligent reflecting surface aided MIMO broadcasting for simultaneous wireless information and power transfer," 2019, *arXiv:1908.04863*. [Online]. Available: http://arxiv.org/abs/1908.04863

[31] E. Basar, "Transmission through large intelligent surfaces: A new frontier in wireless communications," in *Proc. Eur. Conf. Netw. Commun. (EuCNC)*, Valencia, Spain, Jun. 2019, pp. 1–6.

[32] B. Di, H. Zhang, L. Song, Y. Li, Z. Han, and H. V. Poor, "Hybrid beamforming for reconfigurable intelligent surface based multi-user communications: Achievable rates with limited discrete phase shifts," 2019, *arXiv:1910.14328*. [Online]. Available: http://arxiv.org/abs/1910.14328

[33] V. C. Thirumavalavan and T. S. Jayaraman, "BER analysis of reconfigurable intelligent surface assisted downlink power domain NOMA system," in *Proc. Int. Conf. Commun. Syst. Netw. (COMSNETS)*, Jan. 2020, pp. 519–522.

[34] M. Jung, W. Saad, Y. Jang, G. Kong, and S. Choi, "Reliability analysis of large intelligent surfaces (LISs): Rate distribution and outage probability," *IEEE Wireless Commun. Lett.*, vol. 8, no. 6, pp. 1662–1666, Dec. 2019.

[35] E. Bjornson, O. Ozdogan, and E. G. Larsson, "Intelligent reflecting surface versus Decode-and-forward: How large surfaces are needed to beat relaying?" *IEEE Wireless Commun. Lett.*, vol. 9, no. 2, pp. 244–248, Feb. 2020.

[36] M. Di Renzo, K. Ntontin, J. Song, F. H. Danufane, X. Qian, F. Lazarakis, J. de Rosny, D.-T. Phan-Huy, O. Simeone, R. Zhang, M. Debbah, G. Lerosey, M. Fink, S. Tretyakov, and S. Shamai (Shitz), "Reconfigurable intelligent surfaces vs. relaying: Differences, similarities, and performance comparison," 2019, *arXiv:1908.08747*. [Online]. Available: http://arxiv.org/abs/1908.08747
[37] M. O. Hasna and M.-S. Alouini, "End-to-end performance of transmission systems with relays over Rayleigh-fading channels," *IEEE Trans. Wireless Commun.*, vol. 2, no. 6, pp. 1126–1131, Nov. 2003.
[38] S.-I. Chu, "Performance of amplify-and-forward cooperative diversity networks with generalized selection combining over Nakagami-*m* fading channels," *IEEE Commun. Lett.*, vol. 16, no. 5, pp. 634–637, May 2012.
[39] H. Guo, J. Ge, and H. Ding, "Symbol error probability of two-way amplify-and-forward relaying," *IEEE Commun. Lett.*, vol. 15, no. 1, pp. 22–24, Jan. 2011.
[40] S.-I. Chu, "Performance of amplify-and-forward cooperative communications with the N^{th} best-relay selection scheme over Nakagami-m fading channels," *IEEE Commun. Lett.*, vol. 15, no. 2, pp. 172–174, Feb. 2011.
[41] Z. Fang, F. Liang, L. Li, and L. Jin, "Performance analysis and power allocation for two-way amplify-and-forward relaying with generalized differential modulation," *IEEE Trans. Veh. Technol.*, vol. 63, no. 2, pp. 937–942, Feb. 2014.
[42] H. X. Nguyen, H. H. Nguyen, and T. Le-Ngoc, "Amplify-and-forward relaying with m-FSK modulation and coherent detection," *IEEE Trans. Commun.*, vol. 60, no. 6, pp. 1555–1562, Jun. 2012.
[43] H. Yu, W. Tang, and S. Li, "Outage probability and SER of amplify-and-forward cognitive relay networks," *IEEE Wireless Commun. Lett.*, vol. 2, no. 2, pp. 219–222, Apr. 2013.
[44] M. Yan, Q. Chen, X. Lei, T. Q. Duong, and P. Fan, "Outage probability of switch and stay combining in two-way amplify-and-forward relay networks," *IEEE Wireless Commun. Lett.*, vol. 1, no. 4, pp. 296–299, Aug. 2012.
[45] J. Lee, M. Rim, and K. Kim, "On the outage performance of selection amplify-and-forward relaying scheme," *IEEE Commun. Lett.*, vol. 18, no. 3, pp. 423–426, Mar. 2014.
[46] D. Lee and J. H. Lee, "Outage probability for dual-hop relaying systems with multiple interferers over Rayleigh fading channels," *IEEE Trans. Veh. Technol.*, vol. 60, no. 1, pp. 333–338, Jan. 2011.
[47] L. Fan, X. Lei, and W. Li, "Exact closed-form expression for ergodic capacity of amplify-and-forward relaying in channel-noise-assisted cooperative networks with relay selection," *IEEE Commun. Lett.*, vol. 15, no. 3, pp. 332–333, Mar. 2011.
[48] T. A. Lamahewa, P. Sadeghi, and X. Zhou, "On lower bounding the information capacity of amplify and forward wireless relay channels with channel estimation errors," *IEEE Trans. Wireless Commun.*, vol. 10, no. 7, pp. 2075–2079, Jul. 2011.
[49] H. Cui, R. Zhang, L. Song, and B. Jiao, "Capacity analysis of bidirectional AF relay selection with imperfect channel state information," *IEEE Wireless Commun. Lett.*, vol. 2, no. 3, pp. 255–258, Jun. 2013.
[50] Y. Bi and Y. Ding, "Ergodic channel capacity of an amplify-and-forward relay system at low SNR in a generic noise environment," *IEEE Trans. Signal Process.*, vol. 60, no. 5, pp. 2694–2700, May 2012.
[51] I. Z. Kovacs, P. C. F. Eggers, K. Olesen, and L. G. Petersen, "Investigations of outdoor-to-indoor mobile-to-mobile radio communication channels," in *Proc. IEEE 56th Veh. Technol. Conf.*, vol. 1, Sep. 2002, pp. 430–434.
[52] P. S. Bithas, K. Maliatsos, and A. G. Kanatas, "The bivariate double Rayleigh distribution for multichannel time-varying systems," *IEEE Wireless Commun. Lett.*, vol. 5, no. 5, pp. 524–527, Oct. 2016.
[53] C. He and Z. J. Wang, "Closed-form BER analysis of non-coherent FSK in MISO double Rayleigh Fading/RFID channel," *IEEE Commun. Lett.*, vol. 15, no. 8, pp. 848–850, Aug. 2011.
[54] H. Srivastava and J. Choi, "Introduction and preliminaries," in *Zeta and q-Zeta Functions and Associated Series and Integrals*. Amsterdam, The Netherlands: Elsevier, 2012, pp. 1–140.
[55] D. Zwillinger, *CRC Standard Mathematical Tables and Formulae*. Boca Raton, FL, USA: CRC Press, 2003.
[56] I. S. Gradshteyn and I. M. Ryzhik, *Table of Integrals, Series, and Products*, 6th ed. New York, NY, USA: Academic, 2000.
[57] J. Patel and C. Read, *Handbook of the Normal Distribution* (Statistics: A Series of Textbooks and Monographs), 2nd ed. New York, NY, USA: Taylor & Francis, 1996. [Online]. Available: https://books.google.gr/books?id=zoVLF0VF9UYC
[58] M. Abramowitz and I. A. Stegun, *Handbook of Mathematical Functions with Formulas, Graphs, and Mathematical Tables*, 9th ed. New York, NY, USA: Dover, 1972.
[59] A. P. Prudnikov, Y. A. Brychkov, and O. I. Marichev, *Integral Series: More Special Functions*, vol. 3. Boca Raton, FL, USA: CRC Press, 1990.
[60] R. Verma, "On some integrals involving Meijer's G-fucntion of two variables," *Nat. Inst. Sci. India*, vol. 39, nos. 5–6, pp. 509–515, 1966.
[61] A. Hirata, H. Takahashi, R. Yamaguchi, T. Kosugi, K. Murata, T. Nagatsuma, N. Kukutsu, and Y. Kado, "Transmission characteristics of 120-GHz-band wireless link using radio-on-fiber technologies," *J. Lightw. Technol.*, vol. 26, no. 15, pp. 2338–2344, Aug. 1, 2008.
[62] H. Zhang, B. Di, L. Song, and Z. Han, "Reconfigurable intelligent surfaces assisted communications with limited phase shifts: How many phase shifts are enough?" *IEEE Trans. Veh. Technol.*, vol. 69, no. 4, pp. 4498–4502, Apr. 2020.
[63] V. S. Asadchy, M. Albooyeh, S. N. Tcvetkova, A. Díaz-Rubio, Y. Ra'di, and S. A. Tretyakov, "Perfect control of reflection and refraction using spatially dispersive metasurfaces," *Phys. Rev. B, Condens. Matter*, vol. 94, no. 7, Aug. 2016, Art. no. 075142.
[64] M. Mokhtar, A.-A.-A. Boulogeorgos, G. K. Karagiannidis, and N. Al-Dhahir, "OFDM opportunistic relaying under joint transmit/receive I/Q imbalance," *IEEE Trans. Commun.*, vol. 62, no. 5, pp. 1458–1468, May 2014.
[65] E. Soleimani-Nasab, M. Matthaiou, M. Ardebilipour, and G. K. Karagiannidis, "Two-way AF relaying in the presence of co-channel interference," *IEEE Trans. Commun.*, vol. 61, no. 8, pp. 3156–3169, Aug. 2013.
[66] C. Zhong, H. A. Suraweera, A. Huang, Z. Zhang, and C. Yuen, "Outage probability of dual-hop multiple antenna AF relaying systems with interference," *IEEE Trans. Commun.*, vol. 61, no. 1, pp. 108–119, Jan. 2013.
[67] M. Dohler and Y. Li, *Cooperative Communications: Hardware, Channel and PHY*. Hoboken, NJ, USA: Wiley, 2010.
[68] S. Primak, V. Kontorovich, and V. Lyandres, *Stochastic Methods and Their Applications to Communications Stochastic Differential Equations Approach*. West Sussex, U.K.: Wiley, 2004.
[69] A. Papoulis and S. Pillai, *Probability, Random Variables, and Stochastic Processes* (McGraw-Hill Series in Electrical Engineering: Communications and Signal Processing). New York, NY, USA: McGraw-Hill, 2002.
[70] L. Glasser, K. T. Kohl, C. Koutschan, V. H. Moll, and A. Straub, "The integrals in Gradshteyn and Ryzhik. Part 22: Bessel-K functions," *Scientia. A, Math. Sci. New Ser.*, vol. 22, pp. 129–151, Jan. 2012.
[71] J. Proakis, *Digital Communications*, 4th ed. New York, NY, USA: McGraw-Hill, 2001.
[72] J. J. Shynk, *Probability, Random Variables, and Random Processes: Theory and Signal Processing Applications*. Hoboken, NJ, USA: Wiley, 2013.
[73] Wolfram Research. (Oct. 2001). *The Wolfram Functions Site*. [Online]. Available: http://functions.wolfram.com/06.25.21.0131.01
[74] Wolfram Site. (Oct. 2001). *Tree. From MathWorld—A Wolfram Web Resource*. Accessed: Nov. 14, 2019. [Online]. Available: http://functions.wolfram.com/HypergeometricFunctions/Hypergeometric2F1/21/02/02/0001/
[75] S. Kumar, "Exact evaluations of some meijer G-functions and probability of all eigenvalues real for the product of two Gaussian matrices," *J. Phys. A, Math. Theor.*, vol. 48, no. 44, Nov. 2015, Art. no. 445206.
[76] V. S. Adamchik and O. I. Marichev, "The algorithm for calculating integrals of hypergeometric type functions and its realization in REDUCE system," in *Proc. Int. Symp. Symbolic Algebr. Comput. (ISSAC)*, New York, NY, USA, 1990, pp. 212–224.
[77] A. M. Mathai, R. K. Saxena, and H. J. Haubold, *The H-Function: Theory and Applications*. London, U.K.: Springer, 2010.
[78] *The Wolfram Functions Site*. Accessed: May 19, 2020. [Online]. Available: http://functions.wolfram.com/03.04.26.0009.01
[79] G. Watson, *A Treatise Theory Bessel Functions* (Cambridge Mathematical Library). Cambridge, U.K.: Cambridge Univ. Press, 1995. [Online]. Available: https://books.google.gr/books?id=Mlk3FrNoEVoC
[80] (Oct. 2001). *The Wolfram Functions Site*. [Online]. Available: http://functions.wolfram.com/03.04.26.0010.01
[81] (Oct. 2001). *The Wolfram Functions Site*. [Online]. Available: http://functions.wolfram.com/07.34.21.0081.01

ALEXANDROS-APOSTOLOS A. BOULOGEORGOS (Senior Member, IEEE) was born in Trikala, Greece, in 1988. He received the Electrical and Computer Engineering (ECE) (5 year) Diploma degree and the Ph.D. degree in wireless communications from the Aristotle University of Thessaloniki (AUTh), in 2012 and 2016, respectively.

Since November 2012, he has been a member of the Wireless Communications System Group of AUTh, working as a Research Assistant/Project Engineer, in various telecommunication and networks projects. In 2017, he joined the Information Technologies Institute, and in November 2017, he joined the Department of Digital Systems, ICT School, University of Piraeus, where he conducts research in the area of wireless communications. From October 2012 to September 2016, he was a Teaching Assistant at the Department of ECE, AUTh, since February 2017, he has been serving as an Adjunct Lecturer at the Department of ECE, University of Western Macedonia, and as an Visiting Lecturer at the Department of Computer Science and Biomedical Informatics, University of Thessaly. He has authored and coauthored more than 50 technical papers, which were published in scientific journals and presented at prestigious international conferences. Furthermore, he has submitted two (one national and one European) patents. His current research interests spans in the area of wireless communications and networks with emphasis in high frequency communications, optical wireless communications, and communications for biomedical applications.

Dr. Boulogeorgos has been involved as a member of Technical Program Committees in several IEEE and non-IEEE conferences and served as a reviewer for various IEEE journals and conferences. He is also a member of the Technical Chamber of Greece. He received the ''Distinction Scholarship Award'' of the Research Committee of AUTh for the year 2014 and was recognized as an Exemplary Reviewer of the IEEE Communication Letters for 2016 (top 3% of reviewers). Moreover, he was named a Top Peer Reviewer (top 1% of reviewers) in Cross-Field and Computer Science in the Global Peer Review Awards 2019, which was presented by the Web of Science and Publons.

ANGELIKI ALEXIOU (Member, IEEE) received the Diploma degree in electrical and computer engineering from the National Technical University of Athens, in 1994, and the Ph.D. degree in electrical engineering from Imperial College of Science, Technology and Medicine, University of London, in 2000. She is currently a Professor at the Department of Digital Systems, ICT School, University of Piraeus. Since May 2009, she has been a Faculty Member at the Department of Digital Systems, where she conducts research and teaches undergraduate and postgraduate courses in the area of broadband communications and advanced wireless technologies. Prior to this appointment, she was with Bell Laboratories, Wireless Research, Lucent Technologies, (later Alcatel-Lucent, currently NOKIA), Swindon, U.K., first as a member of technical staff, from January 1999 to February 2006, and later as a Technical Manager, from March 2006 to April 2009. Her current research interests include radio interface for 5G systems and beyond, MIMO and high frequencies (mmWave and THz wireless) technologies, cooperation, coordination, and efficient resource management for Ultra Dense wireless networks and machine-to-machine communications, 'cell-less' architectures based on virtualization and extreme resources sharing, and machine learning for wireless systems. She was a co-recipient of the Bell Labs President's Gold Award, in 2002, for contributions to Bell Labs Layered Space-Time (BLAST) project and the Central Bell Labs Teamwork Award, in 2004, for role model teamwork and technical achievements in the IST FITNESS project. She is the Chair of the Working Group on Radio Communication Technologies and of the Working Group on High Frequencies Radio Technologies of the Wireless World Research Forum. She is a member of the Technical Chamber of Greece. She is the Project Coordinator of the H2020 TERRANOVA Project and the Technical Manager of H2020 ARIADNE Project.